



HAL
open science

Molecular underpinnings and environmental drivers of loss of heterozygosity in *Drosophila* intestinal stem cells

Lara Al Zouabi, Marine Stefanutti, Spyridon Roumeliotis, Gwenn Le Meur, Benjamin Boumard, Nick Riddiford, Natalia Rubanova, Mylène Bohec, Louis Gervais, Nicolas Servant, et al.

► To cite this version:

Lara Al Zouabi, Marine Stefanutti, Spyridon Roumeliotis, Gwenn Le Meur, Benjamin Boumard, et al.. Molecular underpinnings and environmental drivers of loss of heterozygosity in *Drosophila* intestinal stem cells. *Cell Reports*, 2023, 42 (12), pp.113485. 10.1016/j.celrep.2023.113485 . hal-04466714

HAL Id: hal-04466714

<https://hal.science/hal-04466714>

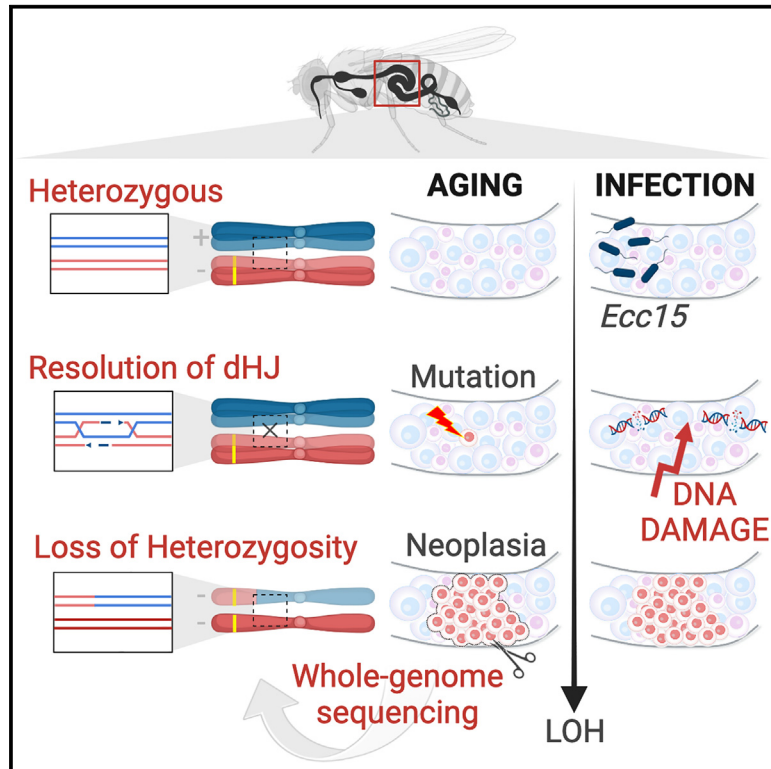
Submitted on 19 Feb 2024

HAL is a multi-disciplinary open access archive for the deposit and dissemination of scientific research documents, whether they are published or not. The documents may come from teaching and research institutions in France or abroad, or from public or private research centers.

L'archive ouverte pluridisciplinaire **HAL**, est destinée au dépôt et à la diffusion de documents scientifiques de niveau recherche, publiés ou non, émanant des établissements d'enseignement et de recherche français ou étrangers, des laboratoires publics ou privés.

Molecular underpinnings and environmental drivers of loss of heterozygosity in *Drosophila* intestinal stem cells

Graphical abstract



Authors

Lara Al Zouabi, Marine Stefanutti, Spyridon Roumeliotis, ..., Louis Gervais, Nicolas Servant, Allison J. Bardin

Correspondence

allison.bardin@curie.fr

In brief

Al Zouabi et al. investigate loss of heterozygosity (LOH) in the adult *Drosophila* midgut. LOH arising in intestinal stem cells increases with age and infection by the bacteria *Ecc15*. They provide insight into the mechanisms of LOH occurring through mitotic recombination, not previously extensively explored in somatic tissues.

Highlights

- Aging ISCs acquire spontaneous LOH events
- The pathogenic bacteria *Ecc15* promotes DNA damage and LOH
- WGS reveals LOH through mitotic recombination
- LOH largely arises from a mechanism consistent with dHJ resolution



Article

Molecular underpinnings and environmental drivers of loss of heterozygosity in *Drosophila* intestinal stem cells

Lara Al Zouabi,^{1,4} Marine Stefanutti,^{1,4} Spyridon Roumeliotis,¹ Gwenn Le Meur,¹ Benjamin Boumard,¹ Nick Riddiford,¹ Natalia Rubanova,^{1,2} Mylène Bohec,³ Louis Gervais,¹ Nicolas Servant,² and Allison J. Bardin^{1,5,*}

¹Genetics and Developmental Biology Department, Institut Curie, PSL Research University, Sorbonne University, CNRS UMR 3215, INSERM U934, 75248 Paris, France

²Bioinformatics, Biostatistics, Epidemiology and Computational Systems Unit, Institut Curie, PSL Research University, INSERM U900, 75005 Paris, France

³ICGex Next-Generation Sequencing Platform, Institut Curie, PSL Research University, 75005 Paris, France

⁴These authors contributed equally

⁵Lead contact

*Correspondence: allison.bardin@curie.fr

<https://doi.org/10.1016/j.celrep.2023.113485>

SUMMARY

During development and aging, genome mutation leading to loss of heterozygosity (LOH) can uncover recessive phenotypes within tissue compartments. This phenomenon occurs in normal human tissues and is prevalent in pathological genetic conditions and cancers. While studies in yeast have defined DNA repair mechanisms that can promote LOH, the predominant pathways and environmental triggers in somatic tissues of multicellular organisms are not well understood. Here, we investigate mechanisms underlying LOH in intestinal stem cells in *Drosophila*. Infection with the pathogenic bacteria, *Erwinia carotovora carotovora* 15, but not *Pseudomonas entomophila*, increases LOH frequency. Using whole genome sequencing of somatic LOH events, we demonstrate that they arise primarily via mitotic recombination. Molecular features and genetic evidence argue against a break-induced replication mechanism and instead support cross-over via double Holliday junction-based repair. This study provides a mechanistic understanding of mitotic recombination, an important mediator of LOH, and its effects on stem cells *in vivo*.

INTRODUCTION

Studies over the past 10 years have brought to light the fact that healthy, adult tissues are composed of a patchwork of diverse genomes arising from somatic mutation of stem and progenitor cells.¹ A major focus of this body of work has been on the acquisition of somatic point mutations, which are easily detected by short-read sequencing-based approaches.^{2–4} Less attention, however, has focused on loss of heterozygosity (LOH) of alleles, which are more challenging to detect in bulk sequencing. LOH is frequently due to copy number changes, removing one allele, but can also be copy neutral (cnLOH), alternatively referred to as uniparental disomy, where two identical alleles are present. While the mechanisms underlying development of cnLOH are not fully understood, chromosome mis-segregation would lead to events affecting whole chromosomes. In contrast, repair of DNA damage mediated by recombination machinery would lead to cnLOH events affecting only chromosome arms or segments of chromosomes.

cnLOH, also known as “mitotic recombination,” was originally identified in classic studies from *Drosophila*⁵ (and reviewed by Studeja and Bardin⁶), although it also has important beneficial

and detrimental consequences on a wide variety of human pathologies. For example, it has been shown to underlie the spontaneous cure of skin diseases such as ichthyosis and epidermolysis bullosa^{7–10} and hematopoietic pathologies like Diamond-Blackfan anemia.^{11–14} In these instances, a heterozygous dominant disease-causing allele is reverted to a wild-type allele upon recombination between homologous chromosomes followed by cell division (reviewed by Revy et al.¹⁵). Mitotic recombination plays a substantial role in both sporadic and familial cancers, particularly problematic for individuals who have germline mutations in adenomatous polyposis coli (*APC*), retinoblastoma, and neurofibromatosis 1.^{16–20} Furthermore, cnLOH has been proposed to represent an important vulnerability in cancers.²¹ A better understanding of the process of mitotic recombination and its impact on healthy tissues and disease pathologies is merited.

Mechanistic insight of the molecular events of mitotic recombination has come largely from studies using budding and fission yeast.^{22–25} In response to a DNA break, homologous recombination can proceed either through the classic double-strand break repair pathway using a double Holliday Junction (dHJ) intermediate,²⁶ via synthesis-dependent strand annealing, or by break-induced replication (BIR) pathway (reviewed by Jinks-Robertson



and Petes,²⁵ Haber,²⁷ and Wu and Malkova²⁸). However, only the classic dHJ and BIR pathways lead to large stretches of LOH along chromosome arms. In the classic dHJ pathway, DNA break repair proceeds via dHJ intermediates, which are often processed by dissolution, creating non-cross-over products.^{29,30} Alternatively, dHJs are resolved via cleavage by endonucleases, which can promote cross-over, leading to LOH of heterozygous alleles.²⁹ BIR, in contrast, involves error-prone synthesis of large portions of chromosomes, resulting in LOH of heterozygous alleles within the copied region.^{25,28} Studies in mammalian cell culture and in *Drosophila* germline cells have provided additional insight into molecular mechanisms of mitotic recombination and indicated a large degree of conservation of enzymes and processes.^{31–37} In particular, *Drosophila* studies revealed that mitotic recombination is normally suppressed by the activity of DNA pol theta-mediated end joining.³⁴ Nevertheless, many questions are outstanding. The roles of repair by the classic dHJ pathway versus BIR in somatic tissues of Metazoa, for example, is currently unknown.

The *Drosophila* adult midgut has become a powerful model system for understanding healthy tissue dynamics as well as cancer initiation, tumor progression and aging (reviewed by Boumard and Bardin³⁸). The intestinal epithelium is composed of differentiated enterocytes (ECs) and enteroendocrine cells (EEs) that are replaced by the asymmetric divisions of intestinal stem cells (ISCs), which are the primary dividing cell type in the midgut.^{39,40} While tissue turnover is slow in unchallenged intestines, ISC proliferation can be rapidly induced by damaging agents, such as pathogenic bacteria,^{41–43} and other damaging agents.^{44,45} The microbiome also impacts the progression of genetically induced tumors.^{46,47} Additionally, induced tumor models in the *Drosophila* intestine have defined cell-autonomous and non-cell-autonomous signals from the surrounding cellular niche that promote tumor growth and survival signals.^{48–59} Thus, the fly gut has provided insight into tumor progression using induced tumor models.

Previously, we demonstrated that the intestine is prone to spontaneous tumor initiation through somatic mutation of ISCs involving gene deletion, chromosome rearrangement, and transposon insertion.^{60–62} Furthermore, our findings suggested that a separate process, likely depending on recombination machinery, can promote LOH.⁶⁰ Here, we take advantage of the fly intestine model to address the underlying molecular mechanisms and drivers of spontaneously arising LOH in adult stem cells.

RESULTS

Spontaneous LOH increases with age

To systematically study mechanisms and frequencies of LOH, we chose a null allele of *Suppressor of Hairless* (*Su(H)*) on Chromosome (Chr) 2L (*Su(H)^{Δ47}*, “*Su(H)-*”) as a marker gene. It encodes a transcriptional factor of the Notch pathway and its loss of function leads to a readily detectable tumor, phenocopying the inactivation of *Notch* with large clones composed of neoplastic ISCs and EE cells.⁶³ The midguts of a majority of aged *Su(H)^{-/+}* female flies presented an overall wild-type appearance, composed of large polyploid ECs with interspersed enteroendocrine (EE cells) and diploid progenitor cells (ISCs and EBs) (Figures 1A and 1B).

Less frequently, aged *Su(H)^{-/+}* midguts were detected with patches of tissue with a *Su(H)* loss-of-function phenotype composed of an accumulation of Delta (DI)-positive ISCs and Prospero⁺ EEs were apparent (Figure 1C). These data suggest that, as we previously demonstrated for other Notch pathway components,⁶⁰ the spontaneous inactivation of the wild-type allele of *Su(H)* occurs during aging representing LOH events.

The frequency of spontaneously arising LOH clones was found to increase with age. While only 0.9% guts had mutant LOH clones in 1-week-old *Su(H)^{-/+}* flies, by 3 weeks of age this rose to 10.8%, and further increased to 73% of midguts by 6 weeks of age (Figure 1D). In addition, 6-week-old wild-type *w¹¹¹⁸* females (+/+) had interspersed ISCs and EEs and lacked aberrant clusters of these cells seen in LOH conditions (Figures 1A and 1D).

Infection with the pathogenic enteric bacteria *Erwinia carotovora carotovora 15* increases LOH

The gut is an organ that responds rapidly to changes in the environment, triggering stem cell proliferation in response to epithelial cell death.⁶⁴ To test the role of external environmental factors in driving LOH, we first wanted to validate that environmental alteration occurring in adult life could indeed affect LOH frequencies in the midgut. X-ray irradiation is known to induce chromosomal breaks that lead to LOH in developing larvae.⁵ Young 1-week-old *Su(H)^{-/+}* flies were irradiated with 40 Gy ionizing radiation (IR) and compared with unirradiated flies at 3 and 6 weeks after IR (Figures 2A–2C). While non-IR treated flies contained 10.8% of guts with spontaneously arising LOH events at 3 weeks, IR-treated flies had a significant increase in LOH events, with 78.4% of midguts containing at least one LOH clones at 3 weeks (Figure 2B). In addition, most IR-treated midguts had multiple events (61.9%). At 6 weeks, almost 100% of IR-treated flies had very large LOH clones, often occupying almost the entire midgut, strongly suggesting clone fusion (Figure 2C). Importantly, these data illustrate that changes to ISCs during adult life can increase LOH frequency in the midgut.

We then wanted to assess whether natural pathogens may impact somatic mutation via LOH in the midgut. The pathogenic bacterial strain *Erwinia carotovora carotovora 15* (*Ecc15*) can infect *Drosophila melanogaster*, cause epithelial damage, and promote ISC proliferation.⁴² As previously reported, *Ecc15* treatment led to an increase in mitotic cells after 24 h of treatment compared with untreated controls (Figure 2D). Punctual exposure of *Su(H)^{-/+}* flies to *Ecc15* during 24 h, once per week for 3 weeks, was performed with midguts assessed at 5 weeks of age. *Ecc15* treatment led to an increase in frequency and number of LOH events compared with controls and an increase in ISCs of the mean intensity of γ H2Av, a mark of DNA damage (Figures 2E and 2F).

We suspected that the effect of *Ecc15* on LOH might be due to the enhanced number of cells divisions, thereby increasing the likelihood of replicative DNA damage. To test whether increased cell division could alter DNA damage and LOH frequency, we modified cell division rates in adult ISCs (DI-GAL4 combined with tub-GAL80ts), using either (1) the overexpression of the cyclin-dependent kinase inhibitor Dacapo (Dap), known to inhibit the G1/S transition and thus reduce cell division,⁶⁵ or (2) the combined overexpression of Cyclin E (CycE) and String (Stg),

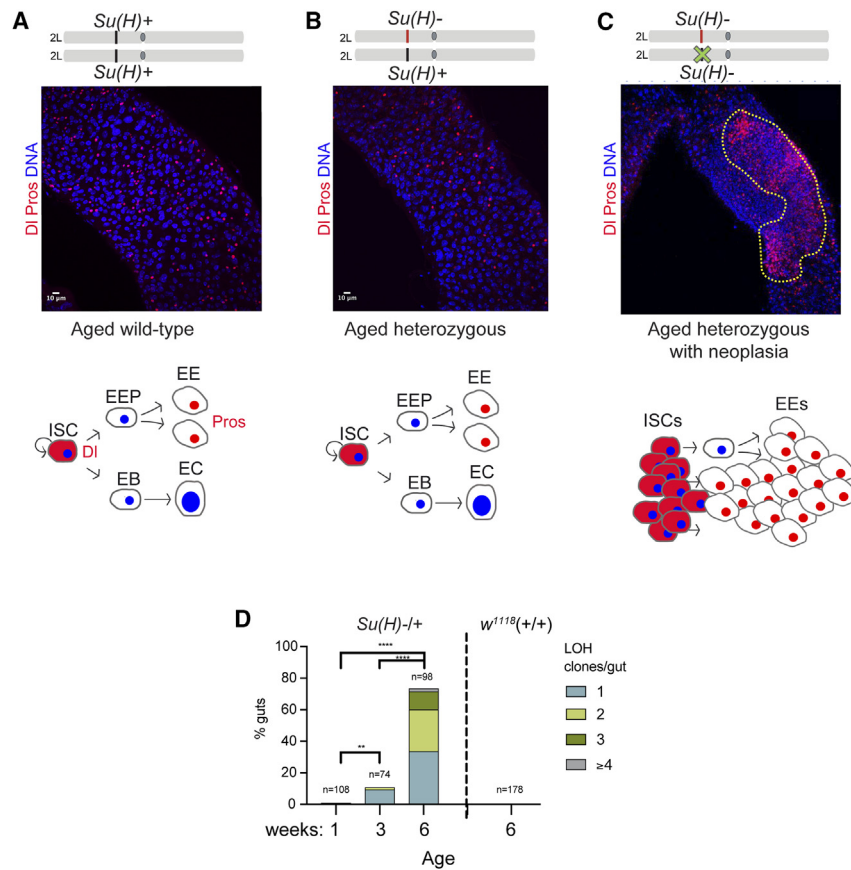


Figure 1. Aging ISCs acquire spontaneous LOH events

(A) A wild-type aged gut at 6 weeks. Polyploid ECs, identified by the large nuclear size (DAPI, in blue), are the primary cell type in the gut and are interspersed with diploid EEs (Prospero [Pros], nuclear red), and ISCs (cytoplasmic puncta of DI staining red). Lower schematic represents ISC lineage: ISCs divide to self-renew and produce EB progenitors that directly differentiate into ECs, representing ~90% of cells in the tissue. Less frequently, around 10% of ISCs, divide to self-renew and produce EE progenitors, which divide once to make two EE cells.

(B) A heterozygous aged gut at 6 weeks. Most of the tissue in the intestines of *Su(H)^{-/-}* flies were like that of wild-type flies, represented by schematic underneath. *Su(H)^{d47}*, a null allele, was used.

(C) An example of a heterozygous *Su(H)^{-/-}* midgut at 6 weeks of age with a neoplastic clone showing loss-of-function phenotype (outlined in yellow), composed of an excess of DI⁺ ISCs and Pros⁺ EEs, shown in the schematic beneath.

(D) The percentage of guts with at least one LOH clone in *Su(H)^{-/-}* midguts at 1, 3 and 6 weeks of ages were compared. Guts with two or more clones are color coded. The 1-week time point was used to calculate statistical significance of proportions of LOH events. No midgut showed a neoplastic LOH clone in aged wild-type intestines. **p < 0.01; ****p < 0.0001 (Fisher's exact test, two-tailed).

previously shown to increase ISC proliferation.⁶⁶ While expression of Dap did not reduce further the basal number of cells in mitosis, the number of LOH events, and quantity of γ H2Av, a mark of DNA damage, were significantly decreased upon Dap expression (Figures 2G–2I and S1). In contrast, upon the combined overexpression of CycE and Stg and increase in PH3⁺ cells accompanied more LOH events and an increase γ H2Av levels in ISCs (Figures 2G–2I and S1). These data suggest that *Ecc15* treatment could potentially impact LOH due to its effect on stem cell proliferation, which may be directly linked to the observed effects on DNA damage.

We then asked whether another pathogenic bacteria resulted in a similar effect on LOH. *Pseudomonas entomophila* (*Pe*) treatment stimulated ISC proliferation as previously reported (Figure 2J).⁴³ *Pe* increased γ H2Av mean intensity in ISCs, though to a lesser extent than *Ecc15*; however, treatment with *Pe* did not significantly alter LOH frequency (Figures 2K, 2L, and S1). Together, our findings demonstrate that environmental changes such as gut enteropathogens can influence the frequency of LOH events, but that they are not all equal in their capacity to induce DNA damage or LOH.

Whole genome sequencing reveals that LOH arises through mitotic recombination

We then wanted to determine the molecular mechanism underlying LOH. While our previous study hinted toward mitotic ho-

mologous recombination as a mechanism because LOH frequency was diminished by balancer chromosomes known to suppress recombination,⁶⁰ other mechanisms could not definitively be excluded. For example, chromosome loss or deletion might lead to LOH. In addition, LOH occurring via cross-over could not be distinguished from that driven by BIR in our previous study.⁶⁰ Finally, a recent study suggested that an unusual chromosome segregation mechanism, “amitosis,” can lead to LOH in the *Drosophila* midgut under conditions of starvation stress.⁶⁷ In the proposed mechanism of amitosis, enteroblast progenitor cells of the gut, after one round of endoreplication while they are 4n ploidy, are thought to undergo a reductive cell division leading to the segregation of two chromosomes originating from the same parent into one daughter cell.⁶⁷

Therefore, to differentiate between these mechanisms, whole genome sequencing (WGS) of *Su(H)* LOH clones was performed to determine the molecular nature of inactivation events (Figures 3A–3C). LOH clones from 5-week-old flies were identified with a GFP reporter of EE cells, which aberrantly accumulate in the tumors as GFP⁺ clusters (*Su(H)^{-/-}; Pros^{V1}-Gal4/UAS-nlsGFP*) (Figure 3B). Genomic DNA was then isolated from the “tumor” mutant clone and “normal” head and Illumina paired-end (150-bp) sequencing was performed on 28 female and 6 male intestinal neoplastic clones along with the head sample from the same fly as a control of the *Su(H)^{-/-}; Pros^{V1}-Gal4/UAS-nlsGFP* genetic background (Table S1 and Figure 3C). Four female samples were excluded from further analysis due to low sequencing coverage after mapping to the *Drosophila*

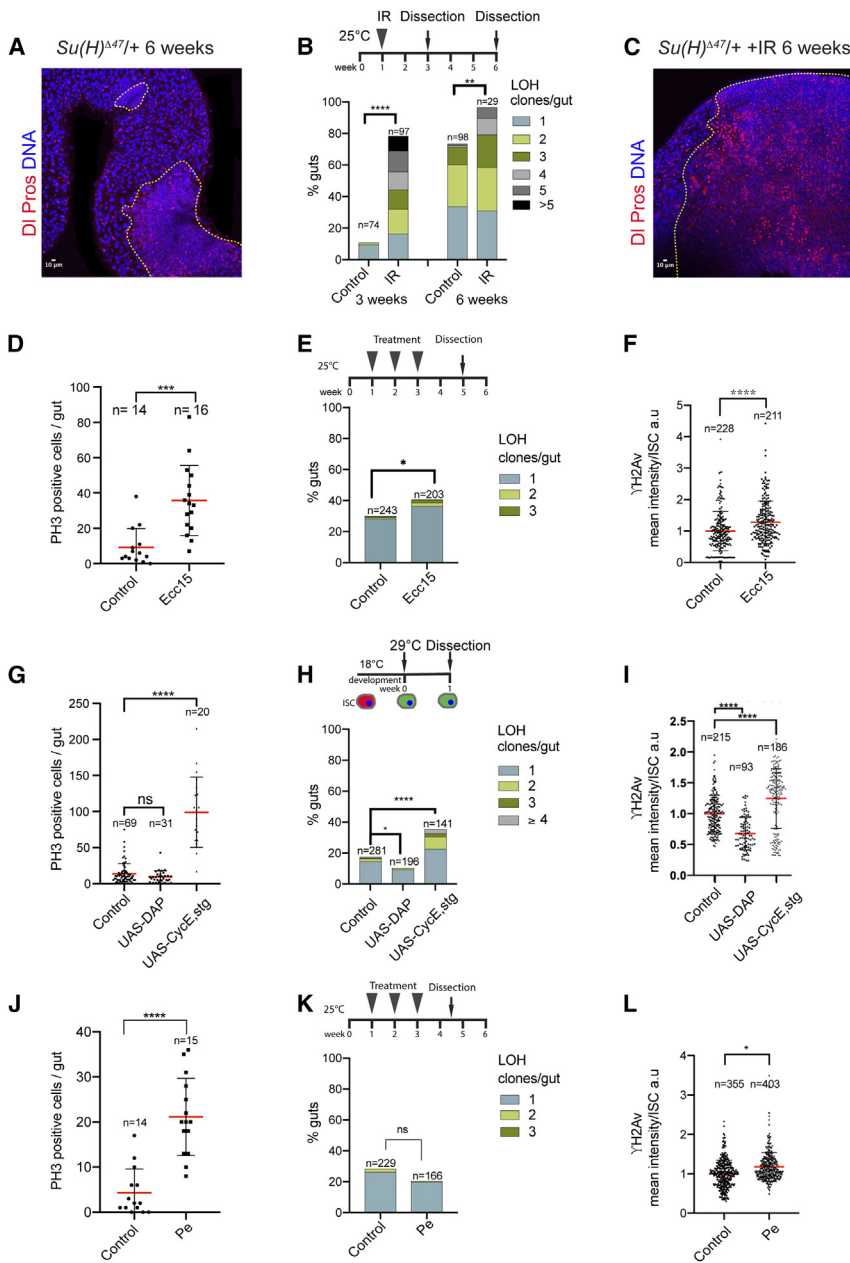


Figure 2. *Ecc15* promotes DNA damage and LOH

(A) Example of 2 LOH events in aged *Su(H)^{-/-}* gut. DI (ISCs, cytoplasmic red), Prospero (Pros) (EEs, nuclear red), DAPI (blue).

(B) A significant increase in LOH percent was found in *Su(H)^{-/-}* flies irradiated at 1 week of age with 40 Gray IR, compared with unirradiated flies at 3 and 6 weeks after IR (Fisher's exact test, two-tailed). Note, control data are also used in Figure 1D.

(C) An example of a large LOH clone in an aged IR-treated *Su(H)^{-/-}* gut outlined in yellow DI (ISCs, cytoplasmic red), Pros (EEs, nuclear red), and DAPI (blue).

(D) Infection of 3- to 5-day-old flies with pathogenic bacteria *Ecc15* stimulates ISC proliferation 24 h after treatment as assessed by phospho-histone H3 (PH3), (t-test with Welch's correction).

(E) Percentage of guts with at least one LOH clone in *Ecc15* treated flies compared with control. Flies were treated for 24 h in weeks 1, 2, and 3 and were dissected in week 5, providing time for recovery to minimize overall toxicity and avoid lifespan reduction (Fisher's exact test, two-tailed).

(F) Infection of 3- to 5-day-old flies with pathogenic bacteria *Ecc15* promoted an increase in γH2Av 24 h after treatment (n = 211, N = 6) compared with control (n = 228, N = 6; t-test with Welch's correction). Data normalized to mean of control, see STAR Methods.

(G) Number of PH3⁺ cells per gut of controls or those upon overexpression of the cell-cycle inhibitor DAP or cell cycle drivers CycE and Stg expressed in stem cells *DI-GAL4* combined with *tub-GAL80ts* for 7 days (t-test with Welch's correction).

(H) Percentage of LOH in midguts of controls and those overexpressing the cell cycle inhibitor DAP or cell cycle drivers CycE and Stg expressed in stem cells *DI-GAL4* combined with *tub-GAL80ts* at 7 days (Fisher's exact test, two-tailed). LOH of the *DI-Gal4* was distinguished from that of *Su(H)* using the UAS-GFP present on Chr3 (see STAR Methods).

(I) Comparison of γH2Av mean intensity (normalized arbitrary units as in F) in ISCs overexpressing DAP (n = 93, N = 5) or cell cycle drivers CycE and Stg in ISCs (n = 186, N = 6) compared with control (n = 215, N = 8). 'n' is the total number of ISCs quantified, 'N' is the number of guts assayed, t-test with Welch's correction.

(J) PH3⁺ cells per gut in 3- to 5-day-old flies after 24 h of *Pe* treatment (t-test with Welch's correction).

(K) Percentage of LOH clones in *Pe* treated flies compared with control (Fisher's exact test, two-tailed).

(L) Comparison of γH2Av mean intensity in ISCs in *Pe* treated (n = 403, N = 5) and control flies (n = 355, N = 8) after 24 h of treatment of 3–5 days old flies (normalized arbitrary units as in F); t-test with Welch's correction. *p < 0.05; **p < 0.01, ****p < 0.0001; not significant. For (D), (F), (G), (I), (J), and (L), the mean value is marked by a red bar and standard deviation by black bars.

genome and removing of duplicate reads (red samples in Table S1). Importantly, the parental genotypes carried a large number of SNPs, used in the bioinformatic analysis detailed below.

To distinguish between different mechanisms of LOH, WGS data of 24 female and 6 male neoplasia samples tumor/normal pairs were analyzed including copy number changes, structural variants, somatic point mutations, and changes to the zygosity of parental SNPs (Figure 3D). In the 24 female samples, we detected no single nucleotide variants or whole chromosomal

copy number changes affecting *Su(H)*, ruling out point mutation and aneuploidy as causes of LOH for these samples (Figures S2A and S2B). One sample showed a large structural variant (deletion) spanning 1.38MB of *Su(H)* (sample F20) (Figures S2C and S2D). In one sample (F28), no LOH or mutation could be found. However, in the majority of samples (22/24 samples), changes in SNP heterozygosity were detected as a shift in zygosity from a variant allele frequency of ~0.5–0.75 or above or 0.25 and below on Chr2L (Figures 4A, 4B, and S2A). As LOH samples have some contaminating

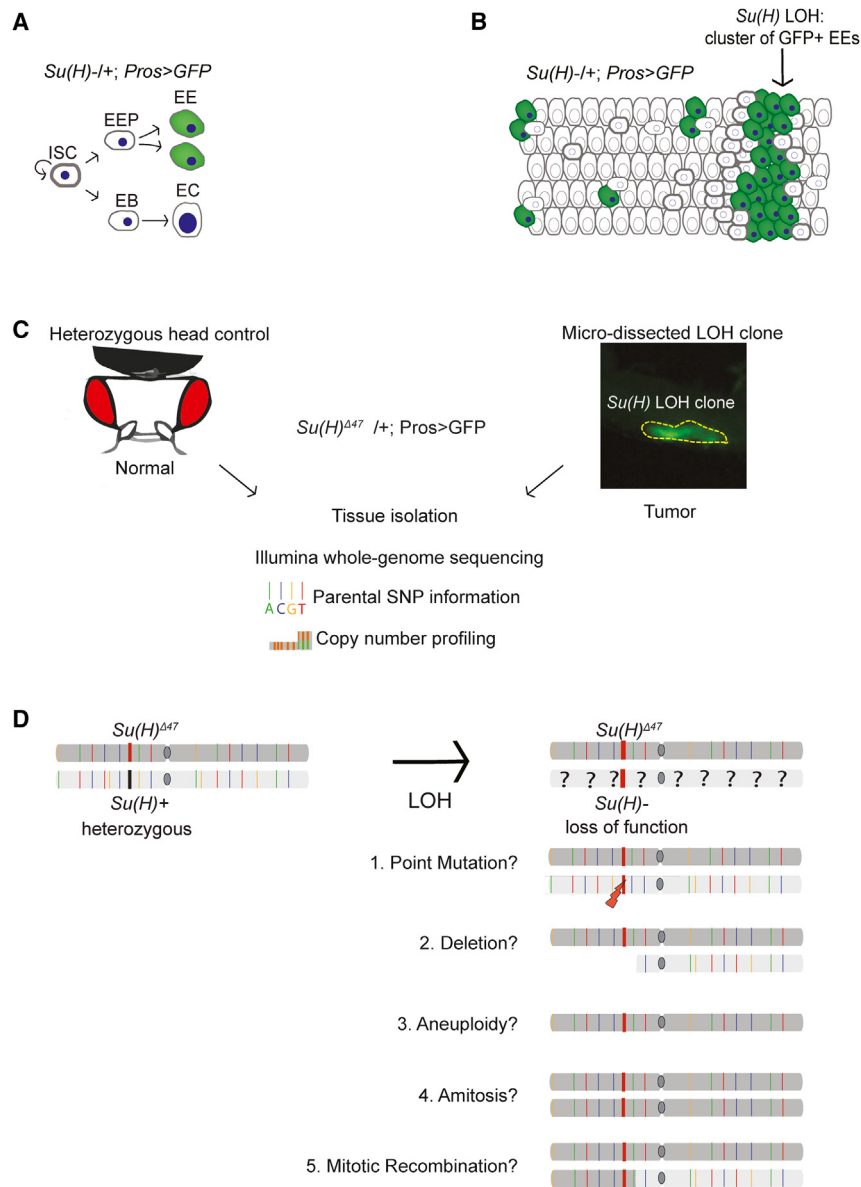


Figure 3. Sequencing setup and analysis predictions

(A) *ProsGal4 UAS-GFP* transgenes drive GFP specifically in EEs allowing for isolation of large GFP⁺ LOH clones composed of ~1,000–5000 cells. (B) Schematic of a *Su(H)* LOH clone recognized by the accumulation (marked by an arrow) of GFP⁺ EEs. (C) The GFP⁺ LOH clones were microdissected along with the head of the same fly for Illumina paired-end sequencing. Of note, the head was used as a control because it contains primarily diploid cells like the neoplastic LOH (composed of ISCs and EEs) as opposed to adjacent gut tissue, which has complex polyploid genomes due to the presence ECs. Germline SNPs, somatic point mutations (single-nucleotide variants [SNVs]), and copy number profiling were assessed. (D) SNP, SNV, and copy number profiling distinguishes between five potential mechanisms by which LOH can arise.

SNPs on Chr2, resulted in LOH of a large portion of the chromosome arm, including the *Su(H)* locus (Figure S3A–A'). The remaining five male neoplastic samples had inactivating deletions of the *Notch* locus located on ChrX, hemizygous in males (Figure S3B–B'), consistent with events that we previously described in wild-type male flies leading to neoplasia.^{62,68} Therefore, in total, mitotic recombination was detected in 23 samples (22 females and 1 male).

These data provide evidence that the primary means of LOH leading to spontaneous neoplasia formation in ISCs is mitotic recombination. Importantly, our data rule out a major contribution of other mechanisms of LOH, including (1) point mutations, (2) deletions, (3) chromosome loss, and (4) amitosis. Furthermore, the long track of LOH extending to the telomere rules out repair mechanisms that result in short tracks of LOH that do not

lead to cross-over, including gap repair, single-strand annealing, and synthesis-dependent strand annealing.²⁷

wild-type adjacent cells, this number does not go to 1 or 0. The positions of LOH invariably arose at locations between the *Su(H)* locus and the centromere 7.5 Mb away and extended throughout the chromosome to the telomere, thereby resulting in LOH of the *Su(H)* locus (Figures 4A, 4B, and 4D; for all 22 samples see Figure 2A). As SNP changes affected only a portion and not the entire chromosome arm, the data supported a mitotic recombination-based mechanism and not amitosis, which would affect the entire chromosome. Further validation of this was obtained taking advantage of the chromosomal position of a UAS-GFP located on Chr2L (28F3–28F5), more telomeric than the *Su(H)* locus on Chr2L (35B), whose expression was lost in LOH clones (Figure S2B).

Additionally, evidence for LOH via mitotic recombination in one of the males samples was also found. A shift in allele frequency of

lead to cross-over, including gap repair, single-strand annealing, and synthesis-dependent strand annealing.²⁷

The Histone Locus Cluster is enriched for sites of mitotic recombination

We next wanted to understand whether there are underlying DNA sequence features that contribute to the DNA damaging event driving mitotic recombination. We were able to map the sites where the recombination occurred in 20 out of the 23 samples, detected as the chromosomal region (sequence) between the first homozygous SNP (from the centromere) and the position of the last heterozygous SNP (from the centromere) in the LOH “tumor” sample (see STAR Methods and Figures 4C and 4D, and Table S2). Recombination sites were mapped from a resolution of 47 bp to 111 kb and had a median size of 1,865 bp

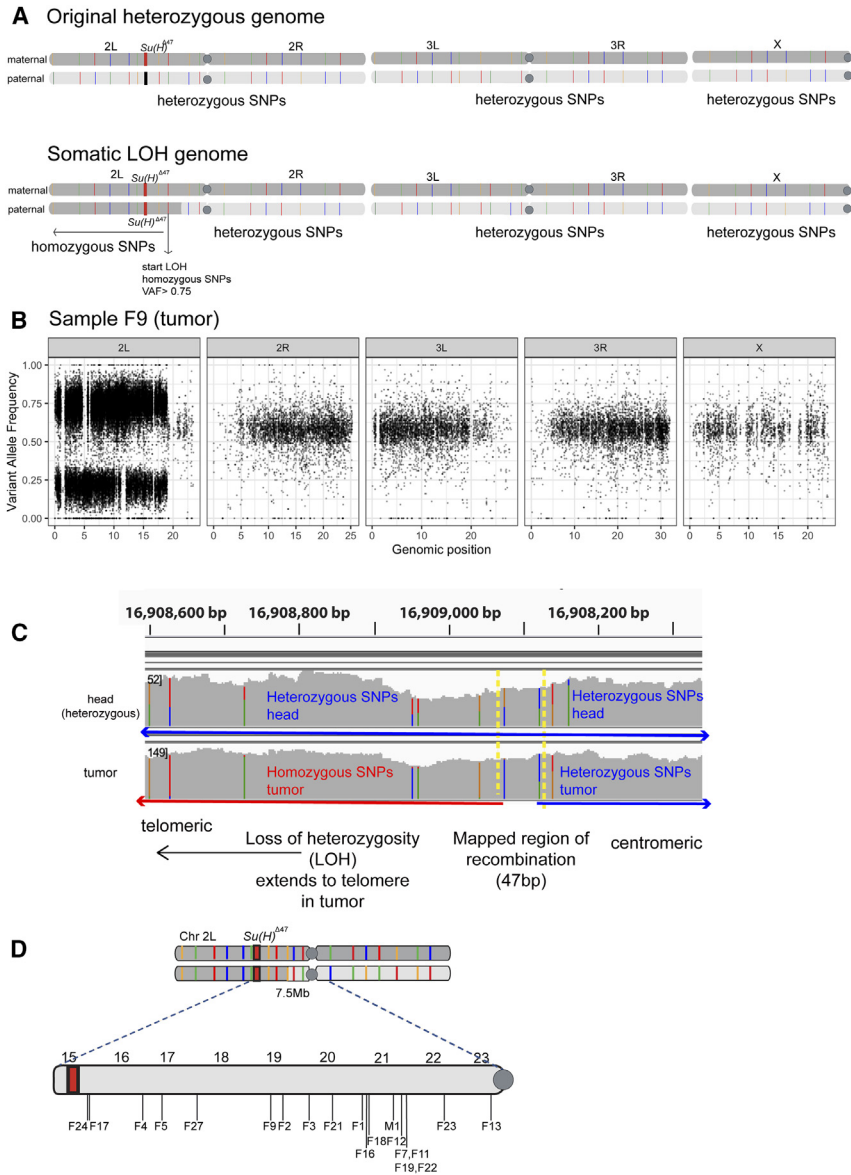


Figure 4. Sequencing *Su(H)* LOH clones reveals that LOH primarily arises through mitotic recombination

(A) A schematic corresponding with the variant allele frequency (VAF) plot below.

(B) A representative VAF plot of a female sample (F9). In this LOH sample, chromosomes 2R, 3L, 3R, and X had heterozygous SNPs, represented at ~0.5 VAF. In contrast, Chr2L has undergone an LOH event, with SNPs becoming homozygous (>0.75%) shown on the left. In a scenario where the tumor purity is 100%, the VAFs in LOH regions should be 1 (100%) or 0; however, given the manual nature of the tumor microdissections, contaminating non-tumor cells make up part of the sequenced tumor resulting in deviations from this.

(C) Integrative Genomics Viewer view of mapping of recombination sites in LOH neoplasias compared with heads. Both head and tumor (LOH) samples show heterozygous SNPs on the right side, seen by colored SNPs each at roughly 50% of the sequencing depth. In contrast, on the left side, these SNPs now become homozygous in the tumor, where they are still heterozygous in the head. Between the yellow lines is the region where recombination took place, mapped within 47 bp of the last heterozygous SNP and the first homozygous SNP in tumor.

(D) All of the mapped recombination sites occurred between *Su(H)* locus (red) and the centromere in female samples (F1–F27) and the male sample M1. Numbers on the chromosome arm correspond with chromosome coordinates.

(Table S2). Three samples had low purity of the neoplastic clone precluding mapping of the region of recombination (see STAR Methods). The position of recombination was then compared with various sequence features. There was no significant overlap with mapped R loops⁶⁹ and predicted sequences for non-B-form DNA such as G-quadruplexes and cruciform DNA, though we did find a significant enrichment for short inverted repeats (SIRS) (Figures 5A–5D).

Interestingly, 4 of the 20 samples had a recombination site that arose within the *Histone Locus Cluster*, a region of 110 kb within the 7.5-Mb region between the centromere and the *Su(H)* locus (Figure 5E). These are only 4 of 20 samples and, thus, should be interpreted with caution. However, the occurrence of recombination sites within this small region (110 kb) was significantly enriched to what was expected using simulated data (Figure 5F). The *Histone Locus Cluster* is an array of 100 copies in tandem

each containing 5 histone genes (H2A, H2B, H3, H4, and H1) (Figure 5E), which has features that could contribute to replication problems. First, it has tandem repeats, which may cause problems for the replication fork. Second, the *Histone Locus Cluster* is also only highly transcribed during S phase when histones are incorporating into newly synthesized DNA,⁷³ which could possibly make it more prone to replication fork collisions with the transcription machinery and lead to DNA damage. Further investigation of the *Histone Locus Cluster* could provide important insight into genomic features potentially driving mitotic recombination from the homologous chromosome.

Rad51 promotes LOH

Our data indicate that mitotic recombination plays a major role in LOH in ISCs. As recombination results from DNA double-strand break repair that uses the Rad51 protein to invade a donor DNA molecule (Figure 6A),^{27,33} we predicted an involvement of the *Drosophila* Rad51 protein Spindle-A (SpnA). We hypothesized that, in absence of SpnA, damaged stem cells would be unable to repair DNA and would consequently die, reducing the number of LOH clones detected. Consistent with this, increased levels of mean γ H2Av intensity were detected in *spnA^{093/spnA⁰⁵⁷}* null mutant ISCs (Figure S4A). LOH frequency decreased from

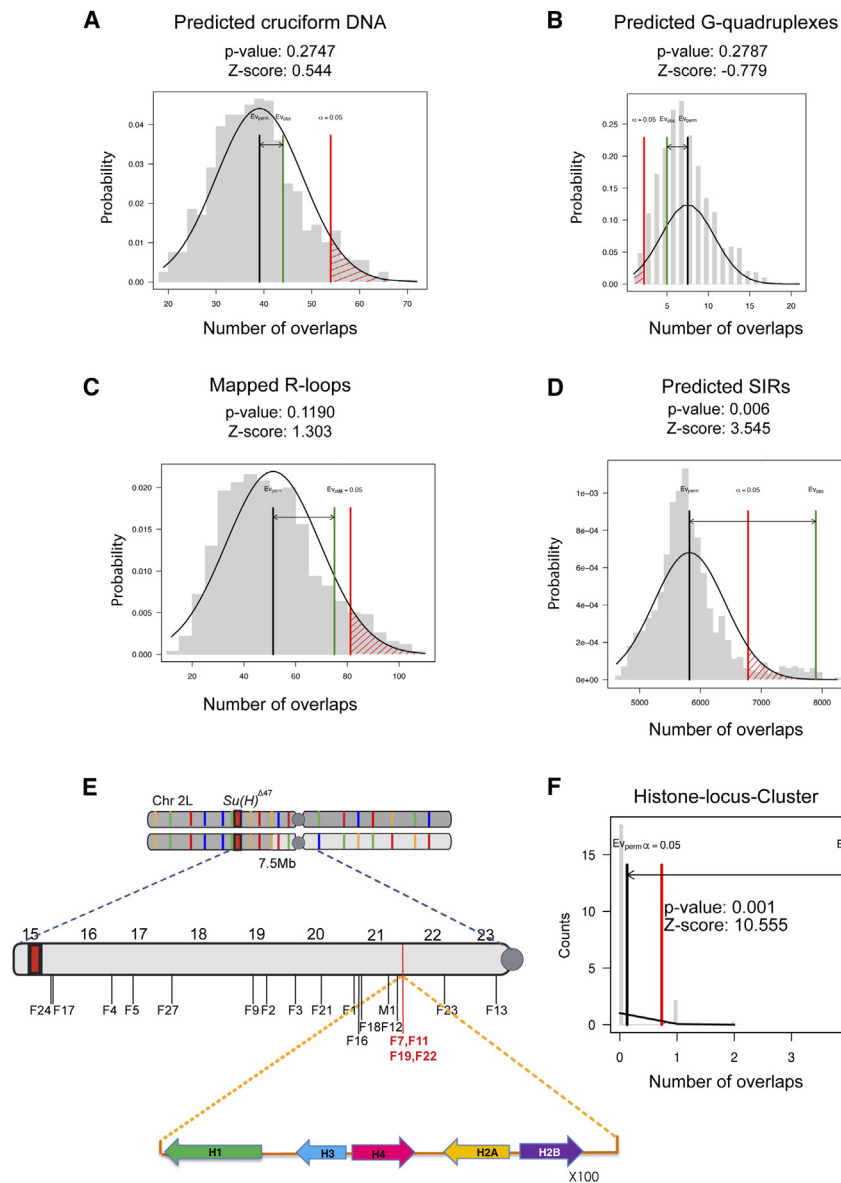


Figure 5. The Histone Locus Cluster: A putative genomic feature driving mitotic recombination

(A–D) Permutation test carried out using RegioneR. Test association between mapped recombination sites and (A) predicted cruciform DNA,⁷⁰ (B) predicted G-quadruplexes,⁷¹ (C) mapped R-loops,⁶⁹ and (D) predicted SIRs.⁷² Shuffles: 1,000 constricted to the region between *Su(H)* and the centromere where recombination can be detected.

(E) Four samples (F7, F11, F19, and F22 shown in red) had recombination sites that occurred within the *Histone Locus Cluster*. Due to the repeat nature, the exact positions could not be mapped within this ~110-kb region. Below the Chr arm is a schematic of the *Histone Locus Cluster*; an array of 100 copies of 5 histone genes.

(F) Permutation test carried out using RegioneR, $p < 0.001$. Test association between mapped recombination sites and the *Histone Locus Cluster*. Shuffles: 1,000 constricted to the region between *Su(H)* and the centromere (where recombination can be detected).

cross-over resulting from a classic double-strand break repair involving a dHJ structure, whose resolution would lead to reciprocal exchange of segments of the homologous chromosomes (Figure 6D), and (2) BIR, in which an error-prone polymerase would copy material directly from the homologous chromosome (Figure 6F). While both mechanisms could lead to long stretches of LOH spanning the chromosome arm and depend on *Rad51*, they differ in their genetic requirements. For this reason, we first decided to test roles of DNA repair proteins specific to each mechanism.

The resolution of dHJ DNA structures relies on resolvases such as Gen and Mus81.^{34,74} While *mus81^{hhe1}* mutant flies did not show consistent differences between mutant and control (Figure S5A), the loss of function of

gen resolvase, in contrast, showed a significant decrease in LOH events, reducing LOH from 59.3% in controls to 42.16% in *gen* mutants (Figure 6E). These data suggest that *gen* is important to promote LOH likely through facilitating DNA repair via dHJ resolution that results in cross-over.

BIR relies on the DNA helicase Pif1, important to unwind the double-strand DNA, thereby allowing to the copying DNA from the homologous donor chromosome^{75–78} (Figure 6F). To test this, *pif1* RNAi was expressed specifically in adult ISCs; no significant change in LOH frequency of *Su(H)*^{-/+} flies was detected (Figures 6G and S4E), suggesting that Pif1 may not play an integral role in the repair giving rise to the LOH events. We, therefore, also examined the genomic features of the chromosomes with LOH.

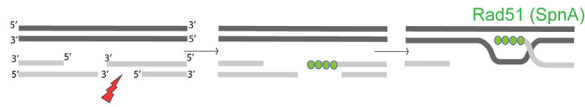
Taking advantage of the high density of parental SNPs, we could assess the regions surrounding the recombination site

32.6% in *Su(H)*^{-/+} controls to 7.5% in *Su(H)*^{-/-}; *spnA*⁰⁹³/*spnA*⁰⁵⁷ null mutants (Figure 6B). No obvious reduction of stem cell numbers or proliferation capacity occurred in *spnA*⁰⁹³/*spnA*⁰⁵⁷ mutants, ruling out the trivial explanation that the ISC population is reduced or becomes senescent (Figures S4B and S4C). Similar to *spnA* mutants, there was a reduction in LOH clones upon knockdown of *Rad51* (*spnA*) using RNAi specifically in adult stem cells (*DI-Gal4*, *tub-Gal80ts*) (Figures 6C and S4D); (see STAR Methods for information on scoring). We conclude that LOH arises in ISCs largely from a Rad51-dependent repair mechanism driving mitotic recombination.

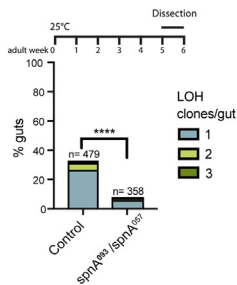
Genetic requirements and molecular signatures support dHJ resolution, leading to cross-over

Two distinct mechanisms of mitotic recombination could explain the long tracts of LOH that were detected in ISCs: (1)

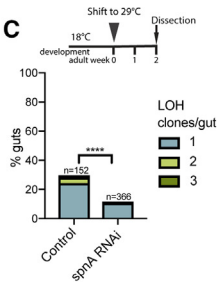
A DSBR



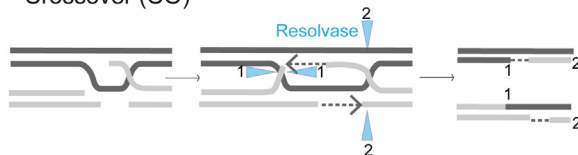
B



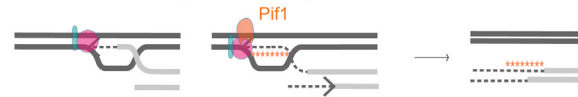
C



D Crossover (CO)



F Break-induced Replication (BIR)



H No mutational pileup akin to BIR repair detected

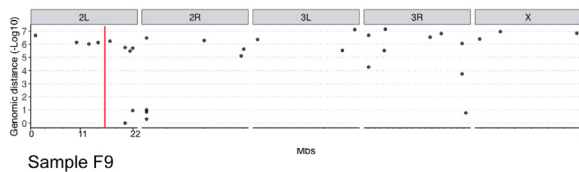


Figure 6. LOH largely arises from a Rad-51-dependent mitotic recombination consistent with dHJ resolution

(A) Double-strand break repair (DSBR) is initiated by 5' end resection and Rad51(SpnA) coating of a 3' end.

(B) Percentage of LOH events in control compared with *spnA* (*Rad51*) null mutant. Fisher's exact test, two-tailed $p < 0.0001$.

(C) Percentage of LOH clones in control compared with a *spnA* (*Rad51*) knockdown in ISCs. Adult flies were shifted to 29°C to induce RNAi for 2 weeks then dissected. (Genotypes: *SpnA* RNAi; *Su(H)^{D47}/UAS-GFP*; *Df^{Gal4} tubGAL80ts/+* vs. *Su(H)^{D47}/UAS-GFP*; *Df^{Gal4} tubGAL80ts/+* control.) Fisher's exact test, two-tailed.

(D) A cross-over (CO) mechanism is mediated by a dHJ and relies on resolvases such as Gen1. Cleavage at sites 1 and 2 result in CO occurring between homologous chromosomes. Depending on the DNA strand, the resulting repaired chromosome can either contain one long LOH tract, or intervening regions of gene conversion nearby the initial breakpoint.

(E) Percentage of LOH events in control compared with *ger²⁴³²⁵* null mutant. Fisher's exact test $p < 0.0001$, two-tailed.

(F) BIR relies on the Pif1 helicase to unwind the template that is used for repair. Repair of the broken chromosome occurs by leading strand copying of the template, and subsequent lagging strand synthesis. It is prone to mutagenesis (stars). The resulting chromosomes are shown, where one is unaltered and one has been repaired by the *de novo* synthesis.

(G) Percentage of LOH clones in control compared with *Pif1* knockdown in ISCs. RNAi was induced in adult ISCs for 2 weeks prior to dissection. Genotypes: *Su(H)^{D47}/UAS-GFP*; *Df^{Gal4} tubGAL80ts/UAS-Pif1 RNAi* vs. *Su(H)^{D47}/UAS-GFP*; *Df^{Gal4} tubGAL80ts/+* control. Fisher's exact test, two-tailed. ns, not significant.

(H) Representative rainfall plot showing no mutation pileup by the mapped recombination site in sample F9 arguing against BIR as a mechanism. The red line indicates the site of mitotic recombination.

for evidence for potential molecular features associated with dHJ resolution or BIR. Of the 20 samples, 16 showed a simple shift from heterozygous to homozygous and seem to be homozygous throughout the chromosome arm (Figures 4C and Table S2). In contrast, 4 of the 20 samples had evidence for intervening tracts where SNPs alternated from heterozygous to homozygous and then homozygous to heterozygous again, followed by heterozygous to homozygous and cross-over (Figures S6A–S6C). For example, sample F1 had an initial shift from heterozygous to homozygous SNPs (at position Chr2L: 20701878–20702379), then 1.5 kb more distally, a region of heterozygosity was again detected, clearly supported by two informative SNPs, followed by again a shift from heterozygous to homozygous throughout the chromosome arm (Figure S6A). Similar shifts from heterozygous to homozygous and homozygous to heterozygous could be detected on three other samples (Figure S6B and S6C, and data not shown for sample F13 where

more than three shifts were detected, suggesting a complex event). These types of tracts could result from predicted outcomes of resolution of dHJ structures, mismatch repair of heteroduplex DNA arising from dHJ structures, or from template switching previously shown to occur in 20% of BIR events.^{25,79}

To further distinguish between mitotic recombination driven by dHJ resolution vs. by BIR, we next assessed the accumulation of somatic point mutations, a hallmark of BIR but not dHJ processing (Deem et al.⁸⁰ and reviewed by Wu and Malkova²⁸). Somatic point mutation (single-nucleotide variant) calling was performed on the genomic samples and none showed evidence of increased mutations near the recombination sites or throughout the arm of Chr2L (Figures 6H and S5B). Therefore, these data argue against BIR as a primary mechanism driving LOH in ISCs.

Altogether, these data support an important role of LOH events being driven by cross-over arising from dHJ resolution, and not BIR. While this mechanism allows repair of double-strand breaks

in stem cells promoting their survival, it leads to LOH of the tumor suppressor *Su(H)* and drives neoplasia initiation.

DISCUSSION

Our findings reveal essential intrinsic and extrinsic factors acting on DNA damage and repair in adult stem cells influencing LOH, an important mechanism of tumor suppressor inactivation. Using WGS and genetic approaches, our data suggest that a major contributor to genome alteration in *Drosophila* ISCs involves mitotic recombination-driven LOH that primarily occurs through a classic HR mechanism, depending on dHJ resolution.

We find that differences in the intestinal microbiota can have distinct impacts on the mutation rate of a tissue. Infection by *Ecc15*, but not *Pe*, altered LOH frequency. *Ecc15* and *Pe* both induce damage to the intestinal epithelium and promote ISC proliferation.^{42,43} Interestingly, we find here that gut enteric pathogenic bacteria can also increase marks of DNA damage. In our experiments, *Ecc15* led to a greater amount of DNA damage than *Pe*, which could explain why *Ecc15* increased LOH frequency but not *Pe*. We also found that under the doses of bacteria that we used, *Ecc15* led to a more pronounced increase in proliferation than *Pe* as assayed 24 h after infection, though it is difficult to assess the cumulative effect of each bacterial treatment on proliferation during the course of the experiment. Of note, the effects of *Ecc15* on DNA damage and LOH can be explained by the increased amount of replication-associated DNA damage as expression of *CycE* and *Stg* in ISCs can also increase LOH frequency and DNA damage. It is possible, however, that other differences between these bacteria or their interaction with the midgut epithelium could also underlie the effect on LOH. Indeed, these bacteria induce overlapping, as well as distinct changes in gene expression in the midgut.⁸¹ In addition, at high doses, *Pe* can inhibit the translation machinery and block ISC proliferation. Consistent with stronger effects on viability, *Pe*-treated flies had reduced 50% survivorship (mean, 23 days) compared with *Ecc15*-treated flies (mean, 31 days), necessitating dissection at 4.5 weeks of age. It is possible that roles in translation or subtle differences in stem cell viability may preclude detections of changes in LOH frequency in *Pe* conditions. Furthermore, it is likely that additional environmental differences contribute to some variation detected during aging in our experiments. In humans, inflammatory bowel disease and colorectal cancer have been linked to alteration of the microbiome.^{82–84} In particular, the NC101 strain of *Escherichia coli* causes DNA damage⁸⁵ and creates a specific mutational signature.⁸⁶ Determining how additional pathogenic bacteria and other changes to environmental conditions affect LOH events may provide strategies for cancer reduction or prevention.

Using high-resolution SNP-based mapping of recombination regions, our study provides direct evidence of mitotic recombination as an underlying mechanism occurring in adult somatic stem cells. Our genetic experiments support these molecular findings as we found reduced LOH in mutant contexts of *Rad51* (*spnA*) and *gen*. Our recent studies illustrated that, in addition to genome alteration by recombination described here, point mutations, deletions, complex structural variants, and transposable element mobility all alter the somatic genome

of ISCs and could, in theory, contribute to LOH.^{61,62} Indeed, we did find one example of LOH driven by a large, 1.38-Mb deletion event. However, our data strongly support mitotic recombination being the primary mechanism by which LOH is generated in ISCs. Importantly, we found no evidence supporting a BIR mechanism as no increase in point mutations was found at LOH regions for the 23 samples that we assessed as would be predicted from previous work.⁸⁰ While our study could only assess those events inducing LOH, it is likely that a much higher number of DNA double-strand breaks are produced but repaired using the sister chromatid, which would be undetectable in our assay. Our findings that dHJ resolution is an important contributor to LOH in somatic tissues suggest that targeting this pathway may be beneficial in patients with germline mutations in recessive tumor suppressor genes or dominant disease genes.

One important question is whether the sites at which recombination arises are simply sites of DNA damage or whether certain underlying genomic features specifically promote cross-over events. Previous studies mapping positions of cross-over, for the most part, have been performed using low-resolution techniques that precluded fine mapping of DNA sequences. To our knowledge, our study is the first high-resolution mapping in a metazoan somatic tissue. In a study of cell lines derived from colorectal cancer driven by LOH of APC, sites of mitotic recombination were resolved to low resolution (~4.5 Mb) and the authors suggest that the sites were non-random and possibly associated with low copy repeats.¹⁶ Previous findings mapped mitotic recombination within the *Drosophila* male germline at low resolution using marker genes and concluded that sites were non-random and provided indirect evidence that they may be linked to problems arising during replication.³³ More precise mapping has been achieved in yeast.^{87–90} These studies found a mitotic recombination hotspot near sites of replication termination, inverted repeats of Ty transposable elements and G-rich quadruplex sequences.^{87–90} While our sample size ($n = 23$) is limited, we did not detect enrichment at mapped cross-over points of these sequences. However, we did find a significant enrichment over what would be predicted by chance at SIRS and the *Histone Locus Cluster*. Our findings of enrichment of SIRS at recombination sites are consistent with previous reports of their ability to stall replication forks and their enrichment at translocation break-points in human cancers.⁷² The *Histone Locus Cluster* encodes ~100 tandem repeats of 5 histone genes (*Histone 1, 2A, 2B, 3A, and 3B*). Why this region has an elevated number of recombination sites than would be predicted by chance is not currently clear; however, we speculate that it is related to the unique features of these genomic locus. One peculiarity of these genes (excluding *Histone H1*) is their exclusive expression at high levels specifically during S phase,⁷³ at which time collisions with DNA polymerase could occur. In addition, this genomic region is also unique in that it forms a nuclear subdomain, the Histone locus body, where specific *Histone* 3' RNA processing occurs, as these are unique in lacking canonical poly A tails. Consistent with DNA damage at the *Histone Locus Cluster*, the *HIST1H* cluster in human B cells is found to acquire marks of γ H2AX.⁹¹ The potential of other genes highly expressed during S phase to be hotspots of DNA damage merits further investigation.

Our study underscores the notion that adult organs are genetic collages, where somatic mutations in adult progenitor cells drive divergent genomes within a common tissue. Given the number of events that we detect here for a marker at one genomic location on 1 out of the 5 major chromosome arms, we can estimate that ~40 LOH events occur per gut for distal genes near the telomeres. As there are ~1,000 ISCs per midgut, we can estimate that 1 in 25 ISCs has an LOH event, raising the likelihood that this mechanism of somatic genetic diversity could alter tissue dynamics during the aging process. Aside from arising somatically in Metazoa, mitotic recombination also occurs in plants as well as diatoms, where it is proposed to contribute to adaptive evolution of clonal populations.^{92,93} Future studies will likely reveal both common as well as species-specific molecular and environmental mediators of mitotic recombination.

Limitations of the study

Our sequencing data here were performed using LOH of *Su(H)* on Chr2L. LOH of other markers on other chromosomes was not assessed at sequencing level resolution. In addition, we are limited in the resolution of the recombination sites by the presence of informative SNPs on the parental lines. Furthermore, due to mapping problems in the repetitive *Histone Locus Cluster*, we could not precisely map recombination sites within this gene cluster.

STAR★METHODS

Detailed methods are provided in the online version of this paper and include the following:

- **KEY RESOURCES TABLE**
- **RESOURCE AVAILABILITY**
 - Lead contact
 - Materials availability
 - Data and code availability
- **EXPERIMENTAL MODEL AND STUDY PARTICIPANT DETAILS**
 - *Drosophila* stocks
- **METHOD DETAILS**
 - *Drosophila* husbandry
 - Bacteria treatments
 - X-Ray induction
 - Immunofluorescence
 - RNAscope for validation of RNAi lines
 - Sample collection for whole-genome sequencing
 - Bioinformatics
- **QUANTIFICATION AND STATISTICAL ANALYSIS**
 - Quantification

SUPPLEMENTAL INFORMATION

Supplemental information can be found online at <https://doi.org/10.1016/j.celrep.2023.113485>.

ACKNOWLEDGMENTS

The authors would like to thank members of the Bardin team, Sarah Lambert, Yohanns Bellaïche, Pierre-Antoine Defossez, Evan Dewey, and Jeff Sekelsky

for helpful discussions and comments on the manuscript. Primary grant support for this work was from Worldwide Cancer Research (WCR 20-0147 grant to A.J.B.). Additional financial support came by grants from Fondation pour la Recherche Médicale (A.B., DEQ20160334928), as well as funding from the program “Investissements d’Avenir” launched by the French Government and implemented by ANR, ANR SoMuSeq-STEM (ANR-16-CE13-0012-01, A.B. and N.S.), ANR ChronoDamage (ANR-20-CE13-0013_01, A.B.), Labex DEEP (ANR-11-LBX-0044), IDEX PSL (ANR-10-IDEX-0001-02 PSL), and ICGex STEM-MITO-REC (A.B.). High-throughput sequencing has been performed by the ICGex NGS Platform of the Institut Curie supported by grants ANR-10-EQPX-03 (Equipex) and ANR-10-INBS-09-08 (France Génomique Consortium) from the Agence Nationale de la Recherche “Investissements d’Avenir” program, by the Cancerpole Ile-de-France and by the SIRIC-Curie program- SIRIC Grant “INCa-DGOS- 465”. Salary support of A.J.B. by CNRS; L.A.-Z. received funding from the European Union’s Horizon 2020 research and innovation program under the Marie Skłodowska-Curie grant agreement No 666003 and the Fondation pour la Recherche Médicale (FRM, FDT201904008016).

AUTHOR CONTRIBUTIONS

L.A.-Z. and A.J.B. designed the study and analyzed the data; L.A.-Z. and M.S. performed the experiments; N. Riddiford developed software and performed most of the bioinformatic analysis, with N. Rubanova performing additional bioinformatic analyses supervised by N.S.; M.B. from the ICGex NGS Platform optimized low-input DNA sequencing; S.R., G.L.M., B.B., and L.G. contributed to experiments; L.A.-Z. and A.J.B. wrote the manuscript with contribution from the other authors.

DECLARATION OF INTERESTS

The authors declare no competing interests.

Received: August 3, 2022

Revised: September 29, 2023

Accepted: November 8, 2023

Published: November 29, 2023

REFERENCES

1. Al Zouabi, L., and Bardin, A.J. (2020). Stem Cell DNA Damage and Genome Mutation in the Context of Aging and Cancer Initiation. *Cold Spring Harbor Perspect. Biol.* 12, a036210.
2. Behjati, S., Huch, M., van Boxtel, R., Karthaus, W., Wedge, D.C., Tamuri, A.U., Martincorena, I., Petljak, M., Alexandrov, L.B., Gundem, G., et al. (2014). Genome sequencing of normal cells reveals developmental lineages and mutational processes. *Nature* 513, 422–425.
3. Martincorena, I., Roshan, A., Gerstung, M., Ellis, P., Van Loo, P., McLaren, S., Wedge, D.C., Fullam, A., Alexandrov, L.B., Tubio, J.M., et al. (2015). Tumor evolution. High burden and pervasive positive selection of somatic mutations in normal human skin. *Science* 348, 880–886.
4. Li, R., Di, L., Li, J., Fan, W., Liu, Y., Guo, W., Liu, W., Liu, L., Li, Q., Chen, L., et al. (2021). A body map of somatic mutagenesis in morphologically normal human tissues. *Nature* 597, 398–403.
5. Stern, C. (1936). Somatic Crossing over and Segregation in *Drosophila Melanogaster*. *Genetics* 21, 625–730.
6. Siudeja, K., and Bardin, A.J. (2017). Somatic recombination in adult tissues: What is there to learn? *Fly (Austin)* 11, 121–128.
7. Jonkman, M.F., Scheffer, H., Stulp, R., Pas, H.H., Nijenhuis, M., Heeres, K., Owaribe, K., Pulkkinen, L., and Uitto, J. (1997). Revertant mosaicism in epidermolysis bullosa caused by mitotic gene conversion. *Cell* 88, 543–551.
8. Jongmans, M.C.J., Verwiël, E.T.P., Heijdra, Y., Vulliamy, T., Kamping, E.J., Hehir-Kwa, J.Y., Bongers, E.M.H.F., Pfundt, R., van Erst, L., van Leeuwen, F.N., et al. (2012). Revertant somatic mosaicism by mitotic

- recombination in dyskeratosis congenita. *Am. J. Hum. Genet.* **90**, 426–433.
9. Choate, K.A., Lu, Y., Zhou, J., Choi, M., Elias, P.M., Farhi, A., Nelson-Williams, C., Crumrine, D., Williams, M.L., Nopper, A.J., et al. (2010). Mitotic recombination in patients with ichthyosis causes reversion of dominant mutations in KRT10. *Science* **330**, 94–97.
 10. Kiritsi, D., He, Y., Pasmooij, A.M.G., Onder, M., Happle, R., Jonkman, M.F., Bruckner-Tuderman, L., and Has, C. (2012). Revertant mosaicism in a human skin fragility disorder results from slipped mispairing and mitotic recombination. *J. Clin. Invest.* **122**, 1742–1746.
 11. Venugopal, P., Moore, S., Lawrence, D.M., George, A.J., Hannan, R.D., Bray, S.C., To, L.B., D'Andrea, R.J., Feng, J., Tirimacco, A., et al. (2017). Self-reverting mutations partially correct the blood phenotype in a Diamond Blackfan anemia patient. *Haematologica* **102**, e506–e509.
 12. Jongmans, M.C.J., Diets, I.J., Quarello, P., Garelli, E., Kuiper, R.P., and Pfundt, R. (2018). Somatic reversion events point towards RPL4 as a novel disease gene in a condition resembling Diamond-Blackfan anemia. *Haematologica* **103**, e607–e609.
 13. Garelli, E., Quarello, P., Giorgio, E., Carando, A., Menegatti, E., Mancini, C., Di Gregorio, E., Crescenzo, N., Palumbo, O., Carella, M., et al. (2019). Spontaneous remission in a Diamond-Blackfan anaemia patient due to a revertant uniparental disomy ablating a de novo RPS19 mutation. *Br. J. Haematol.* **185**, 994–998.
 14. Hirschhorn, R., Yang, D.R., Puck, J.M., Huie, M.L., Jiang, C.K., and Kurlandsky, L.E. (1996). Spontaneous in vivo reversion to normal of an inherited mutation in a patient with adenosine deaminase deficiency. *Nat. Genet.* **13**, 290–295.
 15. Revy, P., Kannengiesser, C., and Fischer, A. (2019). Somatic genetic rescue in Mendelian haematopoietic diseases. *Nat. Rev. Genet.* **20**, 582–598.
 16. Howarth, K., Ranta, S., Winter, E., Teixeira, A., Schaschl, H., Harvey, J.J., Rowan, A., Jones, A., Spain, S., Clark, S., et al. (2009). A mitotic recombination map proximal to the APC locus on chromosome 5q and assessment of influences on colorectal cancer risk. *BMC Med. Genet.* **10**, 54.
 17. Cottrell, S., Bicknell, D., Kaklamani, L., and Bodmer, W.F. (1992). Molecular analysis of APC mutations in familial adenomatous polyposis and sporadic colon carcinomas. *Lancet* **340**, 626–630.
 18. Cavenee, W.K., Dryja, T.P., Phillips, R.A., Benedict, W.F., Godbout, R., Gallie, B.L., Murphree, A.L., Strong, L.C., and White, R.L. (1983). Expression of recessive alleles by chromosomal mechanisms in retinoblastoma. *Nature* **305**, 779–784.
 19. Serra, E., Rosenbaum, T., Nadal, M., Winner, U., Ars, E., Estivill, X., and Lázaro, C. (2001). Mitotic recombination effects homozygosity for NF1 germline mutations in neurofibromas. *Nat. Genet.* **28**, 294–296.
 20. Garcia-Linares, C., Fernández-Rodríguez, J., Terribas, E., Mercadé, J., Pros, E., Benito, L., Benavente, Y., Capellà, G., Ravello, A., Blanco, I., et al. (2011). Dissecting loss of heterozygosity (LOH) in neurofibromatosis type 1-associated neurofibromas: Importance of copy neutral LOH. *Hum. Mutat.* **32**, 78–90.
 21. Nichols, C.A., Gibson, W.J., Brown, M.S., Kosmicki, J.A., Busanovich, J.P., Wei, H., Urbanski, L.M., Curimjee, N., Berger, A.C., Gao, G.F., et al. (2020). Loss of heterozygosity of essential genes represents a widespread class of potential cancer vulnerabilities. *Nat. Commun.* **11**, 2517.
 22. Lee, P.S., Greenwell, P.W., Dominska, M., Gaweł, M., Hamilton, M., and Petes, T.D. (2009). A fine-structure map of spontaneous mitotic crossovers in the yeast *Saccharomyces cerevisiae*. *PLoS Genet.* **5**, e1000410.
 23. Symington, L.S., Rothstein, R., and Lisby, M. (2014). Mechanisms and regulation of mitotic recombination in *Saccharomyces cerevisiae*. *Genetics* **198**, 795–835.
 24. Lisby, M., and Rothstein, R. (2015). Cell biology of mitotic recombination. *Cold Spring Harbor Perspect. Biol.* **7**, a016535.
 25. Jinks-Robertson, S., and Petes, T.D. (2021). Mitotic recombination in yeast: what we know and what we don't know. *Curr. Opin. Genet. Dev.* **71**, 78–85.
 26. Szostak, J.W., Orr-Weaver, T.L., Rothstein, R.J., and Stahl, F.W. (1983). The double-strand-break repair model for recombination. *Cell* **33**, 25–35.
 27. Haber, J.E. (2018). DNA Repair: The Search for Homology. *Bioessays* **40**, e1700229.
 28. Wu, X., and Malkova, A. (2021). Break-induced replication mechanisms in yeast and mammals. *Curr. Opin. Genet. Dev.* **71**, 163–170.
 29. Bizard, A.H., and Hickson, I.D. (2014). The dissolution of double Holliday junctions. *Cold Spring Harbor Perspect. Biol.* **6**, a016477.
 30. West, S.C., Blanco, M.G., Chan, Y.W., Matos, J., Sarbajna, S., and Wyatt, H.D.M. (2015). Resolution of Recombination Intermediates: Mechanisms and Regulation. *Cold Spring Harbor Symp. Quant. Biol.* **80**, 103–109.
 31. LaRocque, J.R., Stark, J.M., Oh, J., Bojilova, E., Yusa, K., Horie, K., Takeda, J., and Jasin, M. (2011). Interhomolog recombination and loss of heterozygosity in wild-type and Bloom syndrome helicase (BLM)-deficient mammalian cells. *Proc. Natl. Acad. Sci. USA* **108**, 11971–11976.
 32. LaFave, M.C., and Sekelsky, J. (2009). Mitotic recombination: why? when? how? where? *PLoS Genet.* **5**, e1000411.
 33. LaFave, M.C., Andersen, S.L., Stoffregen, E.P., Holsclaw, J.K., Kohl, K.P., Overton, L.J., and Sekelsky, J. (2014). Sources and structures of mitotic crossovers that arise when BLM helicase is absent in *Drosophila*. *Genetics* **196**, 107–118.
 34. Carvajal-Garcia, J., Crown, K.N., Ramsden, D.A., and Sekelsky, J. (2021). DNA polymerase theta suppresses mitotic crossing over. *PLoS Genet.* **17**, e1009267.
 35. Kuo, H.K., McMahan, S., Rota, C.M., Kohl, K.P., and Sekelsky, J. (2014). *Drosophila* FANCM Helicase Prevents Spontaneous Mitotic Crossovers Generated by the MUS81 and SLX1 Nucleases. *Genetics* **198**, 935–945.
 36. Moynahan, M.E., and Jasin, M. (1997). Loss of heterozygosity induced by a chromosomal double-strand break. *Proc. Natl. Acad. Sci. USA* **94**, 8988–8993.
 37. Prakash, R., Sandoval, T., Morati, F., Zagalbaum, J.A., Lim, P.X., White, T., Taylor, B., Wang, R., Desclos, E.C.B., Sullivan, M.R., et al. (2021). Distinct pathways of homologous recombination controlled by the SWS1-SWSAP1-SPIDR complex. *Nat. Commun.* **12**, 4255.
 38. Boumard, B., and Bardin, A.J. (2021). An amuse-bouche of stem cell regulation: Underlying principles and mechanisms from adult *Drosophila* intestinal stem cells. *Curr. Opin. Cell Biol.* **73**, 58–68.
 39. Micchelli, C.A., and Perrimon, N. (2006). Evidence that stem cells reside in the adult *Drosophila* midgut epithelium. *Nature* **439**, 475–479.
 40. Ohlstein, B., and Spradling, A. (2006). The adult *Drosophila* posterior midgut is maintained by pluripotent stem cells. *Nature* **439**, 470–474.
 41. Apidianakis, Y., Pitsouli, C., Perrimon, N., and Rahme, L. (2009). Synergy between bacterial infection and genetic predisposition in intestinal dysplasia. *Proc. Natl. Acad. Sci. USA* **106**, 20883–20888.
 42. Buchon, N., Broderick, N.A., Poidevin, M., Pradervand, S., and Lemaitre, B. (2009). *Drosophila* intestinal response to bacterial infection: activation of host defense and stem cell proliferation. *Cell Host Microbe* **5**, 200–211.
 43. Jiang, H., Patel, P.H., Kohlmaier, A., Grenley, M.O., McEwen, D.G., and Edgar, B.A. (2009). Cytokine/Jak/Stat signaling mediates regeneration and homeostasis in the *Drosophila* midgut. *Cell* **137**, 1343–1355.
 44. Biteau, B., Hochmuth, C.E., and Jasper, H. (2008). JNK activity in somatic stem cells causes loss of tissue homeostasis in the aging *Drosophila* gut. *Cell Stem Cell* **3**, 442–455.
 45. Amcheslavsky, A., Jiang, J., and Ip, Y.T. (2009). Tissue damage-induced intestinal stem cell division in *Drosophila*. *Cell Stem Cell* **4**, 49–61.
 46. Ferguson, M., Petkau, K., Shin, M., Galenza, A., Fast, D., and Foley, E. (2021). Differential effects of commensal bacteria on progenitor cell

adhesion, division symmetry and tumorigenesis in the *Drosophila* intestine. *Development* 148.

47. Zhou, J., and Boutros, M. (2020). JNK-dependent intestinal barrier failure disrupts host-microbe homeostasis during tumorigenesis. *Proc. Natl. Acad. Sci. USA* 117, 9401–9412.
48. Campbell, K., Rossi, F., Adams, J., Pitsidianaki, I., Barriga, F.M., Garcia-Gerique, L., Battle, E., Casanova, J., and Casali, A. (2019). Collective cell migration and metastases induced by an epithelial-to-mesenchymal transition in *Drosophila* intestinal tumors. *Nat. Commun.* 10, 2311.
49. Tamamouna, V., Rahman, M.M., Petersson, M., Charalambous, I., Kux, K., Mainor, H., Bolender, V., Isbilir, B., Edgar, B.A., and Pitsouli, C. (2021). Remodelling of oxygen-transporting tracheoles drives intestinal regeneration and tumorigenesis in *Drosophila*. *Nat. Cell Biol.* 23, 497–510.
50. Singh, S.R., Zeng, X., Zhao, J., Liu, Y., Hou, G., Liu, H., and Hou, S.X. (2016). The lipolysis pathway sustains normal and transformed stem cells in adult *Drosophila*. *Nature* 538, 109–113.
51. Bensard, C.L., Wisidagama, D.R., Olson, K.A., Berg, J.A., Krah, N.M., Schell, J.C., Nowinski, S.M., Fogarty, S., Bott, A.J., Wei, P., et al. (2020). Regulation of Tumor Initiation by the Mitochondrial Pyruvate Carrier. *Cell Metabol.* 31, 284–300.e7.
52. Cordero, J.B., Stefanatos, R.K., Myant, K., Vidal, M., and Sansom, O.J. (2012). Non-autonomous crosstalk between the Jak/Stat and Egfr pathways mediates Apc1-driven intestinal stem cell hyperplasia in the *Drosophila* adult midgut. *Development* 139, 4524–4535.
53. Suijkerbuijk, S.J.E., Kolahgar, G., Kucinski, I., and Piddini, E. (2016). Cell Competition Drives the Growth of Intestinal Adenomas in *Drosophila*. *Curr. Biol.* 26, 428–438.
54. Zhai, Z., Kondo, S., Ha, N., Boquete, J.P., Brunner, M., Ueda, R., and Lemaitre, B. (2015). Accumulation of differentiating intestinal stem cell progenies drives tumorigenesis. *Nat. Commun.* 6, 10219.
55. Ngo, S., Liang, J., Su, Y.H., and O'Brien, L.E. (2020). Disruption of EGF Feedback by Intestinal Tumors and Neighboring Cells in *Drosophila*. *Curr. Biol.* 30, 1537–1546.e3.
56. Patel, P.H., Dutta, D., and Edgar, B.A. (2015). Niche appropriation by *Drosophila* intestinal stem cell tumours. *Nat. Cell Biol.* 17, 1182–1192.
57. Zhou, J., Valentini, E., and Boutros, M. (2021). Microenvironmental innate immune signaling and cell mechanical responses promote tumor growth. *Dev. Cell* 56, 1884–1899.e5.
58. Bangi, E., Pitsouli, C., Rahme, L.G., Cagan, R., and Apidianakis, Y. (2012). Immune response to bacteria induces dissemination of Ras-activated *Drosophila* hindgut cells. *EMBO Rep.* 13, 569–576.
59. Zipper, L., Batchu, S., Kaya, N.H., Antonello, Z.A., and Reiff, T. (2022). The MicroRNA miR-277 Controls Physiology and Pathology of the Adult *Drosophila* Midgut by Regulating the Expression of Fatty Acid beta-Oxidation-Related Genes in Intestinal Stem Cells. *Metabolites* 12, 315.
60. Siudeja, K., Nassari, S., Gervais, L., Skorski, P., Lameiras, S., Stofa, D., Zande, M., Bernard, V., Frio, T.R., and Bardin, A.J. (2015). Frequent Somatic Mutation in Adult Intestinal Stem Cells Drives Neoplasia and Genetic Mosaicism during Aging. *Cell Stem Cell* 17, 663–674.
61. Siudeja, K., van den Beek, M., Riddiford, N., Boumard, B., Wurmser, A., Stefanutti, M., Lameiras, S., and Bardin, A.J. (2021). Unraveling the features of somatic transposition in the *Drosophila* intestine. *EMBO J.* 40, e106388.
62. Riddiford, N., Siudeja, K., van den Beek, M., Boumard, B., and Bardin, A.J. (2021). Evolution and genomic signatures of spontaneous somatic mutation in *Drosophila* intestinal stem cells. *Genome Res.* 31, 1419–1432.
63. Bardin, A.J., Perdigoto, C.N., Southall, T.D., Brand, A.H., and Schweisguth, F. (2010). Transcriptional control of stem cell maintenance in the *Drosophila* intestine. *Development* 137, 705–714.
64. Gervais, L., and Bardin, A.J. (2017). Tissue homeostasis and aging: new insight from the fly intestine. *Curr. Opin. Cell Biol.* 48, 97–105.
65. Reis, T., and Edgar, B.A. (2004). Negative regulation of dE2F1 by cyclin-dependent kinases controls cell cycle timing. *Cell* 117, 253–264.
66. Kohlmaier, A., Fassnacht, C., Jin, Y., Reuter, H., Begum, J., Dutta, D., and Edgar, B.A. (2015). Src kinase function controls progenitor cell pools during regeneration and tumor onset in the *Drosophila* intestine. *Oncogene* 34, 2371–2384.
67. Lucchetta, E.M., and Ohlstein, B. (2017). Amitosis of Polyploid Cells Regenerates Functional Stem Cells in the *Drosophila* Intestine. *Cell Stem Cell* 20, 609–620.e6.
68. Siudeja, K., Nassari, S., Gervais, L., Skorski, P., Lameiras, S., Stofa, D., Zande, M., Bernard, V., Frio, T.R., and Bardin, A.J. (2015). Frequent Somatic Mutation in Adult Intestinal Stem Cells Drives Neoplasia and Genetic Mosaicism during Aging. *Cell Stem Cell* 17, 663–674.
69. Alecki, C., Chiwara, V., Sanz, L.A., Grau, D., Arias Pérez, O., Boulier, E.L., Armache, K.J., Chédin, F., and Francis, N.J. (2020). RNA-DNA strand exchange by the *Drosophila* Polycomb complex PRC2. *Nat. Commun.* 11, 1781.
70. Kurahashi, H., Inagaki, H., Yamada, K., Ohye, T., Taniguchi, M., Emanuel, B.S., and Toda, T. (2004). Cruciform DNA structure underlies the etiology for palindrome-mediated human chromosomal translocations. *J. Biol. Chem.* 279, 35377–35383.
71. Paeschke, K., Capra, J.A., and Zakian, V.A. (2011). DNA replication through G-quadruplex motifs is promoted by the *Saccharomyces cerevisiae* Pif1 DNA helicase. *Cell* 145, 678–691.
72. Lu, S., Wang, G., Bacolla, A., Zhao, J., Spitser, S., and Vasquez, K.M. (2015). Short Inverted Repeats Are Hotspots for Genetic Instability: Relevance to Cancer Genomes. *Cell Rep.* 10, 1674–1680.
73. Marzluff, W.F., and Koreski, K.P. (2017). Birth and Death of Histone mRNAs. *Trends Genet.* 33, 745–759.
74. Ho, C.K., Mazón, G., Lam, A.F., and Symington, L.S. (2010). Mus81 and Yen1 promote reciprocal exchange during mitotic recombination to maintain genome integrity in budding yeast. *Mol. Cell* 40, 988–1000.
75. Wilson, M.A., Kwon, Y., Xu, Y., Chung, W.H., Chi, P., Niu, H., Mayle, R., Chen, X., Malkova, A., Sung, P., and Ira, G. (2013). Pif1 helicase and Poldelta promote recombination-coupled DNA synthesis via bubble migration. *Nature* 502, 393–396.
76. Kocak, E., Dykstra, S., Nemeth, A., Coughlin, C.G., Rodgers, K., and McVey, M. (2019). The *Drosophila melanogaster* PIF1 Helicase Promotes Survival During Replication Stress and Processive DNA Synthesis During Double-Strand Gap Repair. *Genetics* 213, 835–847.
77. Bhandari, J., Karg, T., and Golic, K.G. (2019). Homolog-Dependent Repair Following Dicentric Chromosome Breakage in *Drosophila melanogaster*. *Genetics* 212, 615–630.
78. Li, S., Wang, H., Jehi, S., Li, J., Liu, S., Wang, Z., Truong, L., Chiba, T., Wang, Z., and Wu, X. (2021). PIF1 helicase promotes break-induced replication in mammalian cells. *EMBO J.* 40, e104509.
79. Smith, C.E., Llorente, B., and Symington, L.S. (2007). Template switching during break-induced replication. *Nature* 447, 102–105.
80. Deem, A., Keszthelyi, A., Blackgrove, T., Vayl, A., Coffey, B., Mathur, R., Chabes, A., and Malkova, A. (2011). Break-induced replication is highly inaccurate. *PLoS Biol.* 9, e1000594.
81. Chakrabarti, S., Liehl, P., Buchon, N., and Lemaitre, B. (2012). Infection-induced host translational blockage inhibits immune responses and epithelial renewal in the *Drosophila* gut. *Cell host & microbe* 12, 60–70.
82. Li, J., Zhang, A.H., Wu, F.F., and Wang, X.J. (2022). Alterations in the Gut Microbiota and Their Metabolites in Colorectal Cancer: Recent Progress and Future Prospects. *Front. Oncol.* 12, 841552.
83. Gagnaire, A., Nadel, B., Raoult, D., Neeffes, J., and Gorvel, J.P. (2017). Collateral damage: insights into bacterial mechanisms that predispose host cells to cancer. *Nat. Rev. Microbiol.* 15, 109–128.
84. Arthur, J.C. (2020). Microbiota and colorectal cancer: colibactin makes its mark. *Nat. Rev. Gastroenterol. Hepatol.* 17, 317–318.

85. Arthur, J.C., Perez-Chanona, E., Mühlbauer, M., Tomkovich, S., Uronis, J.M., Fan, T.J., Campbell, B.J., Abujamel, T., Dogan, B., Rogers, A.B., et al. (2012). Intestinal inflammation targets cancer-inducing activity of the microbiota. *Science* *338*, 120–123.
86. Pleguezuelos-Manzano, C., Puschhof, J., Rosendahl Huber, A., van Hoeck, A., Wood, H.M., Nomburg, J., Gurjao, C., Manders, F., Dalmasso, G., Stege, P.B., et al. (2020). Mutational signature in colorectal cancer caused by genotoxic pks(+) *E. coli*. *Nature* *580*, 269–273.
87. St Charles, J., and Petes, T.D. (2013). High-resolution mapping of spontaneous mitotic recombination hotspots on the 1.1 Mb arm of yeast chromosome IV. *PLoS Genet.* *9*, e1003434.
88. Yin, Y., and Petes, T.D. (2013). Genome-wide high-resolution mapping of UV-induced mitotic recombination events in *Saccharomyces cerevisiae*. *PLoS Genet.* *9*, e1003894.
89. Yin, Y., Dominska, M., Yim, E., and Petes, T.D. (2017). High-resolution mapping of heteroduplex DNA formed during UV-induced and spontaneous mitotic recombination events in yeast. *Elife* *6*, e28069.
90. Sui, Y., Qi, L., Wu, J.K., Wen, X.P., Tang, X.X., Ma, Z.J., Wu, X.C., Zhang, K., Kokoska, R.J., Zheng, D.Q., and Petes, T.D. (2020). Genome-wide mapping of spontaneous genetic alterations in diploid yeast cells. *Proc. Natl. Acad. Sci. USA* *117*, 28191–28200.
91. Boulianne, B., Robinson, M.E., May, P.C., Castellano, L., Blighe, K., Thomas, J., Reid, A., Müschen, M., Apperley, J.F., Stebbing, J., and Feldhahn, N. (2017). Lineage-Specific Genes Are Prominent DNA Damage Hotspots during Leukemic Transformation of B Cell Precursors. *Cell Rep.* *18*, 1687–1698.
92. Bulankova, P., Sekulic, M., Jallet, D., Nef, C., van Oosterhout, C., Delmont, T.O., Vercauteren, I., Osuna-Cruz, C.M., Vancaester, E., Mock, T., et al. (2021). Mitotic recombination between homologous chromosomes drives genomic diversity in diatoms. *Curr. Biol.* *31*, 3221–3232.
93. Jia, X., Zhang, Q., Jiang, M., Huang, J., Yu, L., Traw, M.B., Tian, D., Hurst, L.D., and Yang, S. (2021). Mitotic gene conversion can be as important as meiotic conversion in driving genetic variability in plants and other species without early germline segregation. *PLoS Biol.* *19*, e3001164.
94. Staeva-Vieira, E., Yoo, S., and Lehmann, R. (2003). An essential role of DmRad51/SpnA in DNA repair and meiotic checkpoint control. *EMBO J.* *22*, 5863–5874.
95. Andersen, S.L., Kuo, H.K., Savukoski, D., Brodsky, M.H., and Sekelsky, J. (2011). Three structure-selective endonucleases are essential in the absence of BLM helicase in *Drosophila*. *PLoS Genet.* *7*, e1002315.
96. Trowbridge, K., McKim, K., Brill, S.J., and Sekelsky, J. (2007). Synthetic lethality of *Drosophila* in the absence of the MUS81 endonuclease and the DmBlm helicase is associated with elevated apoptosis. *Genetics* *176*, 1993–2001.
97. Balakireva, M., Stocker, R.F., Gendre, N., and Ferveur, J.F. (1998). Voila, a new *Drosophila* courtship variant that affects the nervous system: behavioral, neural, and genetic characterization. *J. Neurosci.* *18*, 4335–4343.
98. Zeng, X., Chauhan, C., and Hou, S.X. (2010). Characterization of midgut stem cell- and enteroblast-specific Gal4 lines in *Drosophila*. *Genesis* *48*, 607–611.
99. Gel, B., Díez-Villanueva, A., Serra, E., Buschbeck, M., Peinado, M.A., and Malinverni, R. (2016). regioneR: an R/Bioconductor package for the association analysis of genomic regions based on permutation tests. *Bioinformatics* *32*, 289–291.
100. Xie, C., and Tammi, M.T. (2009). CNV-seq, a new method to detect copy number variation using high-throughput sequencing. *BMC Bioinf.* *10*, 80.
101. Di Tommaso, P., Chatzou, M., Floden, E.W., Barja, P.P., Palumbo, E., and Notredame, C. (2017). Nextflow enables reproducible computational workflows. *Nat. Biotechnol.* *35*, 316–319.
102. Bolger, A.M., Lohse, M., and Usadel, B. (2014). Trimmomatic: a flexible trimmer for Illumina sequence data. *Bioinformatics* *30*, 2114–2120.
103. Ewels, P., Magnusson, M., Lundin, S., and Käller, M. (2016). MultiQC: summarize analysis results for multiple tools and samples in a single report. *Bioinformatics* *32*, 3047–3048.
104. Danecek, P., Bonfield, J.K., Liddle, J., Marshall, J., Ohan, V., Pollard, M.O., Whitwham, A., Keane, T., McCarthy, S.A., Davies, R.M., and Li, H. (2021). Twelve years of SAMtools and BCFtools. *GigaScience* *10*, giab008.

STAR★METHODS

KEY RESOURCES TABLE

REAGENT or RESOURCE	SOURCE	IDENTIFIER
Antibodies		
Mouse anti-Delta ECD (1:1000)	DSHB	Cat# c594.9b, RRID: AB_528194
Mouse anti-Prospero (1:1000)	DSHB	Cat# Prospero (MR1A-c) RRID: AB_528440
Chicken anti-GFP (1:2000)	Invitrogen	Cat# A10262 RRID: AB_2534023
Rabbit anti-Histone H2AvD pS137 (1:1000)	Rockland	Cat# 600-401-914 RRID: AB_828383
Rabbit anti-PH3 (1:2000)	Millipore	Cat# 06-570 RRID: AB_310177
Chemicals, peptides, and recombinant proteins		
RNAscope probes – Pif1	ACD biotech	NM_001298658.1
RNAscope probes – SpnA	ACD biotech	NM_079844.4
Critical commercial assays		
QIAquick PCR Purification Kit	Qiagen	Cat# 28104
QIAmp DNA Micro Kit	Qiagen	Cat# 56304
RNAscope Multiplex Fluorescent Reagent Kit v2	ACD	Cat#323100
Nextera XT DNA Library Prep Kit	Illumina	Cat# FC-121-1030
KAPA HyperPlus Kit	ROCHE	Cat#07962380001
KAPA Library Quantification Kits	ROCHE	Cat#07960140001
Deposited data		
NCBI BioProject database	NCBI: PRJNA858414	https://www.ncbi.nlm.nih.gov/bioproject/
Experimental models: Organisms/strains		
<i>Drosophila</i> : UAS-GFPnls	Bloomington Drosophila Stock Center	RRID:BDSC_4776
<i>Drosophila</i> : SpnA ⁰⁹³ mutant	M. McVey (Staeva-Vieira, 2003) ⁹⁴	N/A
<i>Drosophila</i> : SpnA ⁰⁵⁷ mutant	M. McVey (Staeva-Vieira, 2003) ⁹⁴	N/A
<i>Drosophila</i> : w[1118]	M. McVey	N/A
<i>Drosophila</i> : Gen[z4325]	J. Sekelsky (Andersen, 2011) ⁹⁵	N/A
<i>Drosophila</i> : mus81[nhe1]	J. Sekelsky (Trowbridge, 2007) ⁹⁶	N/A
<i>Drosophila</i> : pros ^{voila} -GAL4	J. De Navascués (Balakireva, 1998) ⁹⁷	N/A
<i>Drosophila</i> : Su(H) ^{A47}	F. Schweisguth	RRID:BDSC_51215
<i>Drosophila</i> : UAS-DAP	B. Edgar (Reis, 2004) ⁶⁵	N/A
<i>Drosophila</i> : UAS-CycE,UAS-stg	B. Edgar (Kohlmaier, 2015) ⁶⁶	N/A
<i>Drosophila</i> : tubGAL80ts DI-GAL4	B. Edgar (Zeng, 2010) ⁹⁸	N/A
<i>Drosophila</i> : Rad51 (spnA)RNAi	VDRC	#13362
<i>Drosophila</i> : Pif1RNAi	VDRC	#34533
<i>Drosophila</i> : engrailed-GAL4 UAS-GFP	Y. Bellaiche	N/A
<i>Pseudomonas entomophila</i>	B. Lemaitre (Jiang et al., 2009) ⁴³	N/A

(Continued on next page)

Continued

REAGENT or RESOURCE	SOURCE	IDENTIFIER
<i>Erwinia carotovora carotovora</i> 15 (Ecc15)	B. Lemaitre (Buchon et al., 2009) ⁴²	N/A
Software and algorithms		
Prism 9	GraphPad Software	RRID:SCR_002798
Fiji	NIH	RRID:SCR_002285
bwa-mem version 0.7.17	H. Li	arXiv:1303.3997v2 [q-bio.GN]
FastQC	S. Andrews	http://www.bioinformatics.babraham.ac.uk/projects/fastqc
bamstats	bamstats	https://biopet.github.io/bamstats/1.0.1/index.html
multiqc	multiqc	https://doi.org/10.1093/bioinformatics/btw354
SAMtools	SAMtools https://www.htslib.org/	Gigascience. 2021; 10(2). https://doi.org/10.1093/gigascience/giab008
VarScan2 version 2.4	Varscan	https://github.com/dkoboldt/varscan/releases
Lohcator	This paper	https://github.com/nriddiford/nf-lohicator/blob/master/bin/lohicator.py
Mosdepth	Mosdepth, B. Pedersen	https://github.com/brentp/mosdepth
CNVPlotteR	This paper	https://github.com/nriddiford/cnvPlotteR.git
Winlow	This paper	https://github.com/nriddiford/winlow
RegioneR	(Gel B, 2016) ⁹⁹	https://github.com/bernatgel/regioneR
CNV-seq	(Xie, 2009) ¹⁰⁰	https://github.com/hliang/cnv-seq

RESOURCE AVAILABILITY

Lead contact

Further information and requests for resources and reagents should be directed to and will be fulfilled by the lead contact, Allison Bardin (allison.bardin@curie.fr).

Materials availability

This study did not generate new unique reagents.

Data and code availability

DNaseq data have been deposited with links accession number NCBI BioProject database: PRJNA858414 (<https://www.ncbi.nlm.nih.gov/bioproject/>).

- Microscopy data reported in this paper will be shared by the **lead contact** upon request.
- The code used in this study, derived is at <https://github.com/nriddiford/nf-lohicator>, <https://github.com/nriddiford/alleleFreqs>, <http://www.bioinformatics.babraham.ac.uk/projects/fastqc>, bamstats <https://biopet.github.io/bamstats/1.0.1/index.html>; <https://github.com/brentp/mosdepth> and is publicly available. DOIs are listed in the **key resources table**.
- Any additional information required to reanalyze the data reported in this paper is available from the **lead contact** upon request.

EXPERIMENTAL MODEL AND STUDY PARTICIPANT DETAILS

Drosophila stocks

The following fly stocks and alleles were used in this study: From the Bloomington stock center: *UAS-GFPnls* (BL 4776). The following stocks were generous gifts: *spnA⁰⁹³*, *spnA⁰⁵⁷*, *w¹¹¹⁸* (M. McVey), *Gen^{Z4325}*, *mus81^{nhe1}* (J. Sekelsky), *Pros^{V1}Gal4* (J. de Navascués), *Su(H)⁴⁴⁷* (F. Schweisguth), *UAS-DAP*, *UAS-CycE* *UAS-stg*, and *tubGAL80ts DI-GAL4* (B. Edgar). From the Vienna *Drosophila* Resource Center (VDRC): *Rad51(spnA) RNAi* (VDRC 13362), *Pif1 RNAi* (VDRC 34533), *engrailed-Gal4 UAS-GFP (Y Bellaiche)*. For all experiments of LOH, the second chromosomes assayed for LOH were identical between the controls and experimental samples.

METHOD DETAILS

Drosophila husbandry

For standard aging of experiments female flies were maintained at 25°C on a standard rich medium composition. Adult progeny were collected at 25°C over 3–4 days. Females were aged with males in the same cage (plastic cages 1 cm diameter, 942 mL), 400–600 flies/cage, and treated as indicated below with bacteria. Freshly yeasted food was provided in petri dishes every 1–2 days. Flies were transferred every 7 days without CO₂ anesthesia to clean cages. Dead flies were scored upon each food change to assess survival rates. Female flies were dissected at 5–6 weeks unless otherwise indicated. Paired control cages were always done with each experimental condition to mitigate the inherent biological variation between experiments that occurs during the course of aging.

For experiments in the genetic background *Su(H)⁴⁴⁷/UAS-GFP; DI-Gal4 tub-GAL80ts/+* used to drive stem cell specific expression in the ISC, due to the *DI-Gal4* driver: Crosses were maintained at 18°C on standard medium, flies were also maintained at 18°C during development and metamorphosis. Newly eclosed flies were collected over 5–7 days. Flies were maintained at 29°C thereafter. The shift to 29°C induced ISC specific UAS-driven transgene as the Gal80 repressor is temperature-sensitive. Flies were dissected after 1 week for *UAS-DAP*, *UAS-CycE*, *UAS-stg* or after 2 weeks at 29°C for *spnA RNAi*, *mus81 RNAi*, *Pif1 RNAi*.

Bacteria treatments

Adult *Su(H)⁴⁴⁷/+* flies were treated for 24 h on filter paper soaked with *Ecc15* or *Pe* or control solution (see below) covering sugar agar (1.5%) plates. *Ecc15* and *Pe* treatment: a 1:1 mix of OD 200 bacterial culture and 5% sucrose. Control: a 1:1 mix of LB and 5% sucrose. Treatment was repeated once per week for 3 weeks, followed by a 1-week-recovery before dissection at 5 weeks. Proliferation response was assayed by phospho-histone 3 staining 24 h after treatment in young 3–5 day-old flies.

X-Ray induction

1 week old flies were placed in the X-ray generator CIXD and exposed to 40 Gy at the RadeXp facility at Institut Curie.

Immunofluorescence

Midgut fixation and immunofluorescence staining were performed as described previously described in.⁶³ Adult female midguts were dissected in PBS and then fixed at room temperature (RT) for 2 h in 4% paraformaldehyde. Guts were trimmed and incubated in PBS 50% glycerol for 30 min before equilibration in PBS 0.1% Triton X-100 (PBT) to clean the lumen. Fixed and cleaned guts were then washed in PBT for at least 30 min before addition of primary antibodies (overnight at 4°C or 3–5 h at RT). After at least 30 min wash, secondary antibodies were incubated 3–5 h before DAPI staining (1 mg/ml) and mounted in 4% N-propyl-galate, 80% glycerol.

The following primary antibodies were used: mouse anti-Delta extra-cellular domain (1/1000; DSHB C594.9b 10X concentrate), mouse anti-Pros (1/1000; DSHB MR1A-c 10X concentrate); chicken anti-GFP (1/2000, Invitrogen #A10262), rabbit anti-PH3, (1:1000; Millipore #06–570 lot 3746384), mouse anti-γH2Av (1:100; DSHB #UNC93–5.2.1 10X concentrate).

Imaging was performed using Zeiss LSM900 and LSM780 confocal microscopes and epifluorescence widefield microscope at the Curie Institute imaging facility with serial optical sections taken at 1 μm intervals (512X512 or 1024X1024) using 20X or 40X oil objectives through the whole-mounted posterior midguts. Maximum projections of 5–11 sections were used for illustration purposes.

RNAscope for validation of RNAi lines

smFISH using RNAscope technology from ACD biotech, with probes against *Pif1* & *SpnA* (13ZZ Made-To-Order Probes) was performed to visualize *Pif1* & *SpnA* mRNA in the wing imaginal disc. RNAscope Probes were designed by ACD biotech: against *Pif1* (accession number NM_001298658.1) targeting nucleotides 1085–1374 and 1721–1978 and against *SpnA* (accession number NM_079844.4) targeting nucleotides 42–606, respectively. Genomic regions covered by RNAi constructs were avoided in the design. RNAscope was performed in an Eppendorf tube. Control larvae (*w¹¹¹⁸*) or those of the genotypes *engrailed-Gal4, UAS-GFP; UAS-RNAi pif1* or *engrailed-Gal4, UAS-GFP; UAS-RNAi spnA* were used. Larvae were dissected in PBS and fixed in 4% paraformaldehyde in PBS for 30 min. Fixed larvae were washed with PBS and then with PBT (PBS containing 0.03% Triton X-100). Fixed larvae were dehydrated at RT (room temperature) in a series of 25, 50, 75 and 100% methanol in PBT. Larvae were rehydrated at RT in a series of 75, 50, 25, 0% methanol in PBT. Larvae were treated with protease using ProteaseIII (RNAscope Multiplex Fluorescent Reagent Kit v2; ACD, #323100) at 40°C for 5 min. After washing with PBT, hybridization using probes against *Pif1* & *SpnA* was performed overnight at 40°C. The following day, larvae were washed with RNAscope wash buffer, provided by the manufacturer. Fluorescent signal was developed using RNAscope Fluorescent Multiplex Reagent Kit according to the manufacturer's instructions. Larvae were incubated overnight at 4°C with a GFP chicken antibody (Invitrogen #A10262) at a dilution of 1:200 in PBT. After washing with PBT, larvae were incubated for 2h at RT with an anti-chicken-488) at a dilution of 1:1000 in PBT. DNA was counterstained with DAPI. Wing discs were dissected and mounted for imaging. Images of wing discs were obtained using a Zeiss LSM900 confocal microscope (section thickness 1 μm).

Sample collection for whole-genome sequencing

Su(H)⁴⁴⁷/+; Pros^{V1}Gal4; UAS-nlsGFP were used to visually identify midguts containing LOH neoplasias. The region of the LOH neoplasia was manually microdissected. An estimate of 50–80% purity of the LOH neoplasia can be achieved. These neoplastic

LOH tumors were dissected together with the fly head. Genomic DNA was isolated using QIAamp DNA MicroKit (Qiagen) according to the manufacturer's instructions.

Library preparation

Library preparation was performed with the Nextera XT kit and KAPA Hyper Plus ROCHE kit by the NGS facility of the Institut Curie. Samples were sequenced on one full flow cell (1600M clusters) on the NovaSeq in a paired-end 150bp mode.

Nextera XT Sample Prep Kit (Illumina) was used to prepare DNA sequencing libraries from 0.5 ng of genomics DNA. A step of enzymatic tagmentation with Nextera transposome was done to fragment DNA and add adapter sequences (Unique Dual Indexing strategy). A final amplification of the library was then performed with 12 cycles. After qPCR quantification (KAPA library quantification Kit, Roche), sequencing were performed on the Illumina NovaSeq 6000 using 2 x 150 cycles to get ~40 M paired-end reads per sample.

KAPA Hyper Plus Kits (Roche) was used to prepare DNA sequencing libraries from 1.3 ng of genomics DNA. A first step of enzymatic fragmentation of 20 min at 37°C was done. An end-repair and A-tailing step on dsDNA fragments have produced end-repaired dsDNA fragments. A ligation overnight with the adapters (Unique Dual Indexing strategy) and a final amplification of the library was then performed with 15 cycles. After qPCR quantification (KAPA library quantification Kit, Roche), sequencing were performed on the Illumina NovaSeq 6000 using 2 x 150 cycles to get ~40 M paired-end reads per sample.

Bioinformatics

Analysis of whole-genome sequencing data

Sequencing analysis of LOH samples was performed using custom scripts implemented in the Nextflow¹⁰¹ pipeline nf-lohcator <https://github.com/nriddiford/nf-lohcator>.

Briefly, adapter sequences were removed using trimmomatic 0.39.¹⁰² Trimmed reads were aligned to release 6.12 of the *Drosophila melanogaster* reference genome (FlyBase) using bwa-mem version 0.7.17 (Li H, 2013, arXiv:1303.3997v2 [q-bio.GN]). Fastqc (Andrews, D. (2010)) FastQC: A Quality Control Tool for High Throughput Sequence Data [Online]. Available online at: <http://www.bioinformatics.babraham.ac.uk/projects/fastqc>, bamstats (<https://biopet.github.io/bamstats/1.0.1/index.html>) and multiqc¹⁰³ were used to provide quality control files.

Alignment files were sorted and indexed using SAMtools¹⁰⁴ followed by the generation of pileup output summarizing the base calls of aligned reads to the reference sequence using mpileup command in SAMtools for each sample. VarScan2 version 2.4 (<https://github.com/dkoboldt/varscan/releases>) was then run on pileups generated. "Lohcator", a custom python script <https://github.com/nriddiford/nf-lohcator/blob/master/bin/lohicator.py> developed in the lab was then ran to identify shifts in zygosity for each tumor sample and to create bed files to facilitate identification of the start and end of LOH for each sample.

VAF representation

VAFs were plotted with alleleFreqs: <https://github.com/nriddiford/alleleFreqs> using the LOH calls from VarScan2.

Rainfall plots

To generate rainfall plots in, filtering was carried out by using the "high quality" somatic calls produced by VarScan2.

We specified minimum coverage of 20 for both the tumor and normal sample and a somatic p value < 0.05. These calls were represented on rainfall plots. Some samples showed no SNVs and are thus not represented in the [Figure S5B](#).

Mapping of regions of recombination

First, on IGV, we confirmed that at this region, all the informative SNPs in the head were heterozygous and homozygous in the tumor. Using a tool we have developed to identify regions of LOH in matched tumor normal pairs (nf-lohcator, see above), we were able to determine where the first homozygous SNP (from the centromere) was located; we then located the first heterozygous SNP on IGV relative to that for the mitotic recombination events. It is important to note that both coverage and tumor purity play an important role in confidently mapping these regions, with more emphasis placed on purity. We determined values for both coverage and purity for each mapped region (see [Table S1](#)). We were unable to map the region of recombination for 3 samples (Samples F8, F10 and F26) because of EC contamination. These samples however allowed us to benchmark what is deemed "too impure" for the mapping of regions of recombination.

Association of mapped breakpoints with genomic regions

To assess whether mapped breakpoints were enriched for the *Histone Locus-Cluster* and other genomic features ([Figure 5](#)), permutation tests were performed using regioneR⁹⁹ to determine the significance of the overlap between sequence features and our mapped breakpoint regions. In order to compare observed counts between real and shuffled data, we restricted permutations to within the genomic locus where mitotic recombination can be detected between the *Su(H)* locus and the centromere chr2L:15039488–23512838, and performed 10,000 permutations.

Calculating coverage

Mosdepth was used to calculate genome-wide sequencing coverage with default parameters (<https://github.com/brentp/mosdepth>).

Copy number analysis

Copy number analysis was performed using a read-depth-based approach with CNV-seq.¹⁰⁰ CNVPlotter <https://github.com/nriddiford/cnvPlotter.git> was then used to generate copy number plots.

Calculating EC contamination

The approach described in⁶² and implemented in <https://github.com/nriddiford/winlow> was used to determine the likely contamination of tumor samples with EC cells (Table S2).

QUANTIFICATION AND STATISTICAL ANALYSIS

Quantification

When possible, quantification was carried out blind. Results quantified are pooled data from either 3 biological replicates or 4 biological replicates.

LOH scoring

LOH events in females heterozygous for *Su(H)* were scored as clusters of at least 20 Delta and/or Prospero positive diploid cells. We note that experimental variation is detected between experiments (likely due to additional environmental factors) and therefore, paired control cages were always done with each experimental condition.

Scoring of *Su(H)* LOH clones in *DI-Gal4* background using UAS-GFP

In experiments using the genetic background *Su(H)^{Δ47}/UAS-GFP; DI-GAL4/+* two types of neoplastic LOH clone could arise: those where *Su(H)* is inactivated and those where *DI* undergoes LOH as *DI-GAL4* is a loss of function allele of *DI*, also a *Notch* signaling component. We distinguished between these two possibilities by taking advantage of a UAS-GFP transgene located on Chr2L more distal on the chromosome arm to *Su(H)*. Therefore, LOH through recombination of *Su(H)* results in neoplastic clones that are GFP negative. These events were scored. In contrast, LOH resulting from other events including mitotic recombination of 3R leading to *DI* LOH, are GFP+. These events were scored, but not counted in the analysis. Statistical analysis for the proportion of LOH clones was carried out in Prism using Fisher's exact test (two-tailed) was performed and significant values were reported as: * $p < 0.05$, *** $p < 0.001$, **** $p < 0.0001$, ns = not significant.

PH3 quantification

PH3 positive cells in the midgut were counted using the epifluorescence microscope. Statistical analysis for the comparing number of PH3+ cells per midgut was carried out in Prism using a t test with Welch's correction and significant values were reported as: * $p < 0.05$, *** $p < 0.001$, **** $p < 0.0001$, ns = not significant.

γ H2Av quantification

16 bit images were acquired on the LSM900 confocal microscope. Maximum Z-projection of 11 sections of 1 μ m apart were generated for all images on ImageJ (FIJI version 1.0). Nuclear γ H2Av intensity in the ISCs was measured. To normalize the data, the mean value of the control was used to divide each value of control and experimental condition. Statistical analysis for the comparing the mean γ H2Av intensity in the ISCs was performed in Prism on the normalized arbitrary units using t test with Welch's correction and significant values were reported as: * $p < 0.05$, *** $p < 0.001$, **** $p < 0.0001$, ns = not significant.

Cell Reports, Volume 42

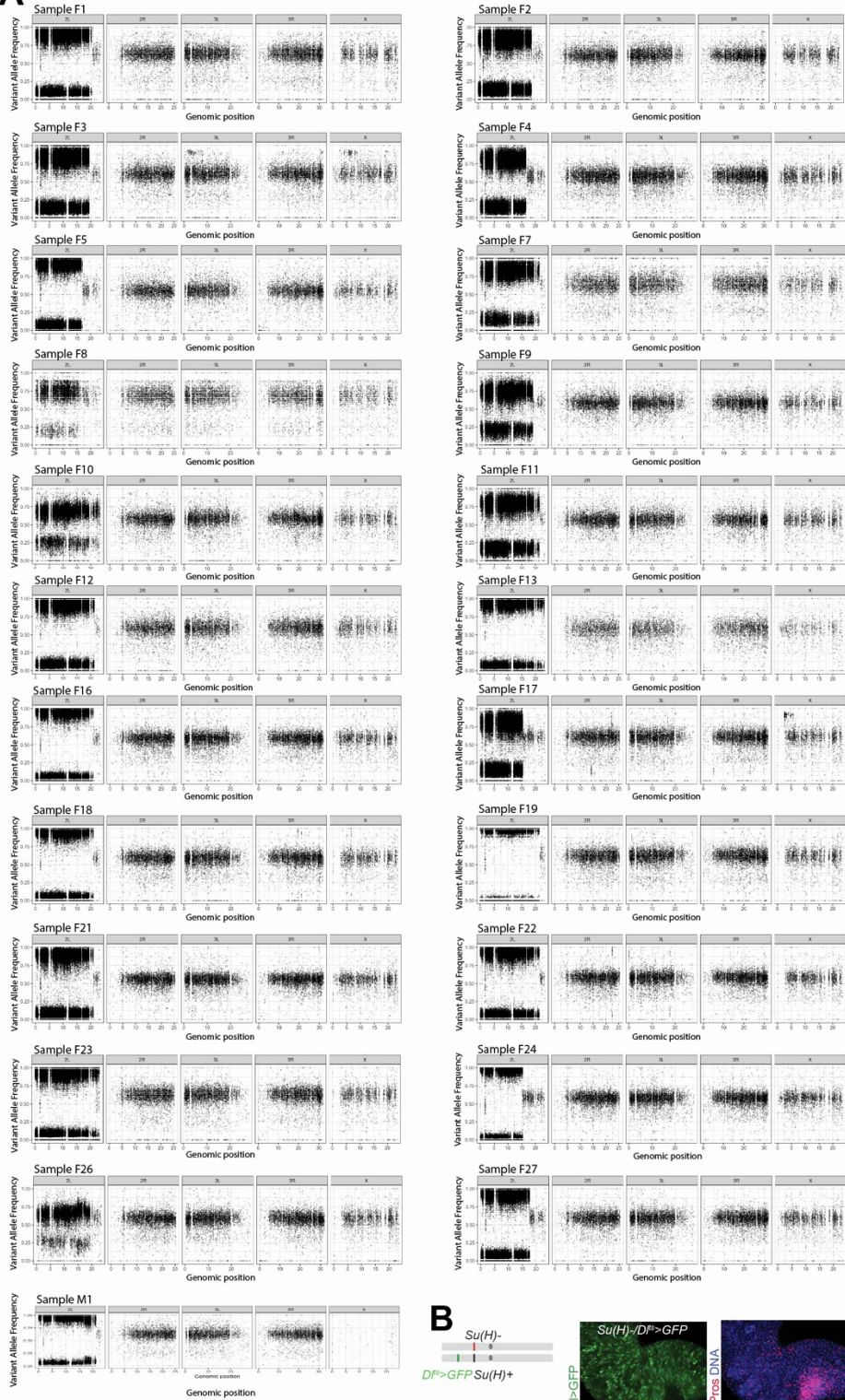
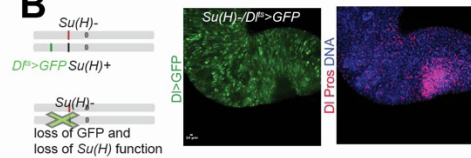
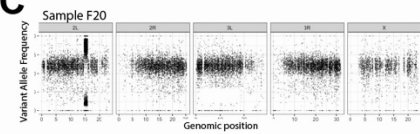
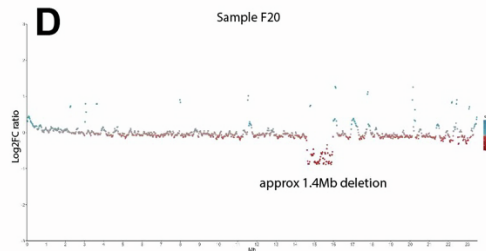
Supplemental information

**Molecular underpinnings and environmental
drivers of loss of heterozygosity in *Drosophila*
intestinal stem cells**

Lara Al Zouabi, Marine Stefanutti, Spyridon Roumeliotis, Gwenn Le Meur, Benjamin Boumard, Nick Riddiford, Natalia Rubanova, Mylène Bohec, Louis Gervais, Nicolas Servant, and Allison J. Bardin

Supplementary Figure 1 (related to Figure 2): DNA damage signals upon cell cycle alteration and bacterial infection

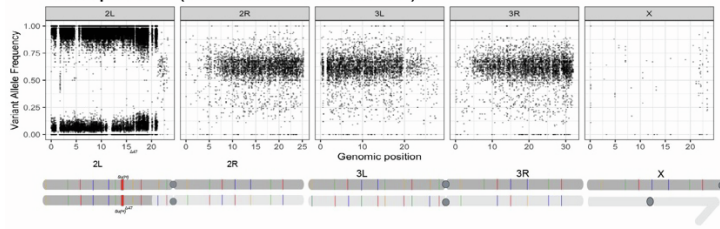
(A) Nuclear γ H2Av intensity in the ISCs was measured in control guts, guts overexpressing *DAP* and guts overexpressing cell cycle drivers *CycE* and *Stg* using *DI-GAL4* combined with *tub-GAL80^{ts}* for 7 days. γ H2Av in white, DI and Pros in red, GFP in green, DAPI marking DNA in blue. ISCs were identified as DI positive, GFP positive. See Figure 2 for quantification. **(B)** Nuclear γ H2Av intensity in the ISCs was measured in control guts and guts infected with *Ecc15* after 24 hour treatment of 3-5 day old flies. (γ H2Av in white, DI and Pros in red, GFP in green, DAPI marking DNA in blue). ISCs were identified as DI positive, GFP positive. **(C)** Nuclear γ H2Av intensity in the ISCs was measured in control guts and guts infected with *Pe* after 24 hour treatment of 3-5 day old flies. (γ H2Av in white, DI and Pros in red, GFP in green, DAPI marking DNA in blue). ISCs were identified as DI positive, GFP positive.

A**B****C****D**

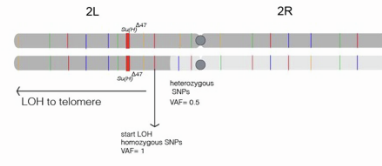
Supplementary Figure 2 (related to Figure 3): Evidence for LOH driven by Mitotic Recombination on Chr2L

(A) Variant allele frequency plots of samples supporting LOH of chromosome (Chr) 2L, with SNPs becoming homozygous (VAF>0.75). Samples F6, F14, F15 and F25 were excluded because of low coverage. **(B)** The genetic background *Su(H)^{D47}/UAS-GFP; Df^{Gal4}/+* was used to drive stem cell specific expression in the ISC, due to the *Df^{Gal4}* driver. Neoplastic LOH clones where *Su(H)* is inactivated resulted in GFP negative clones due to the loss of the UAS-GFP transgene located on Chr 2L more distal on the chromosome arm to *Su(H)* via mitotic recombination (GFP in green, DI and Pros in red, DAPI marking DNA in blue). **(C)** VAF plot of sample F20 showing a shift in allele frequency on Chr 2L where there is a deletion. **(D)** Copy number plot showing a large drop in coverage (approximately 1.4 Mb) in the tumor relative to the head control in sample F20.

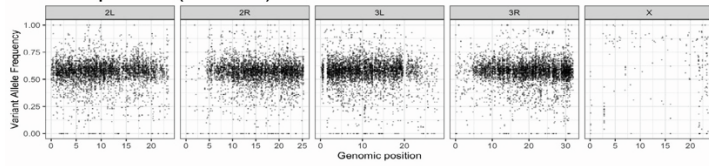
A Sample M1 (mitotic recombination)



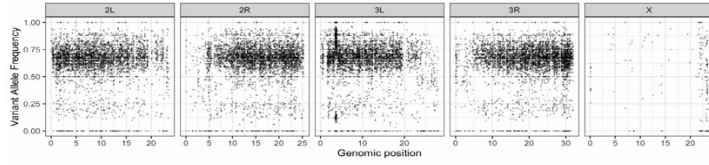
A'



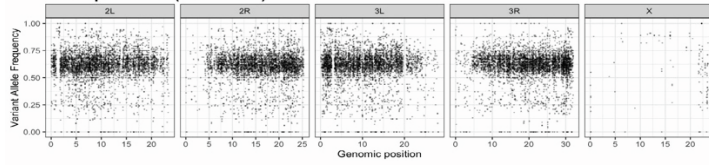
B Sample M2 (SV in *N*)



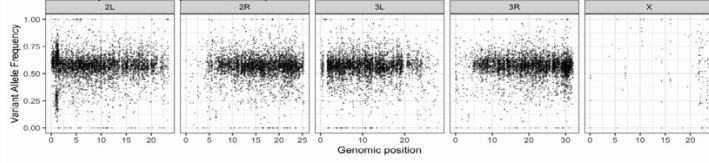
Sample M3 (SV in *N*)



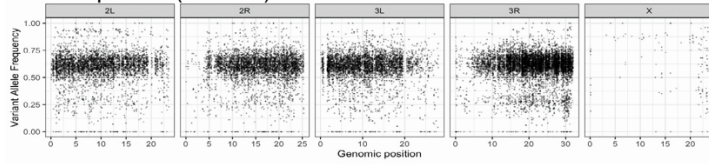
Sample M4 (SV in *N*)



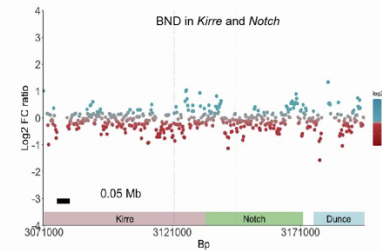
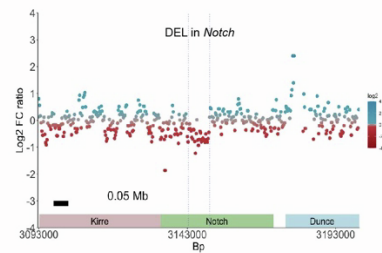
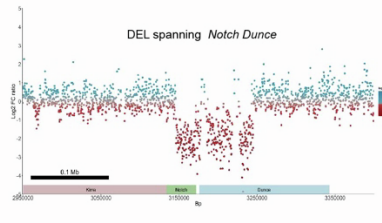
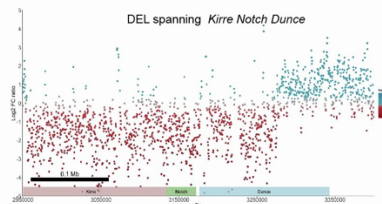
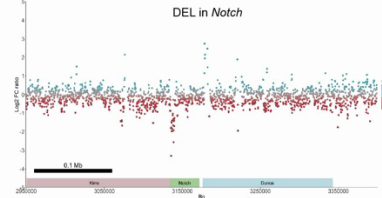
Sample M5 (SV in *N*)



Sample M6 (SV in *N*)

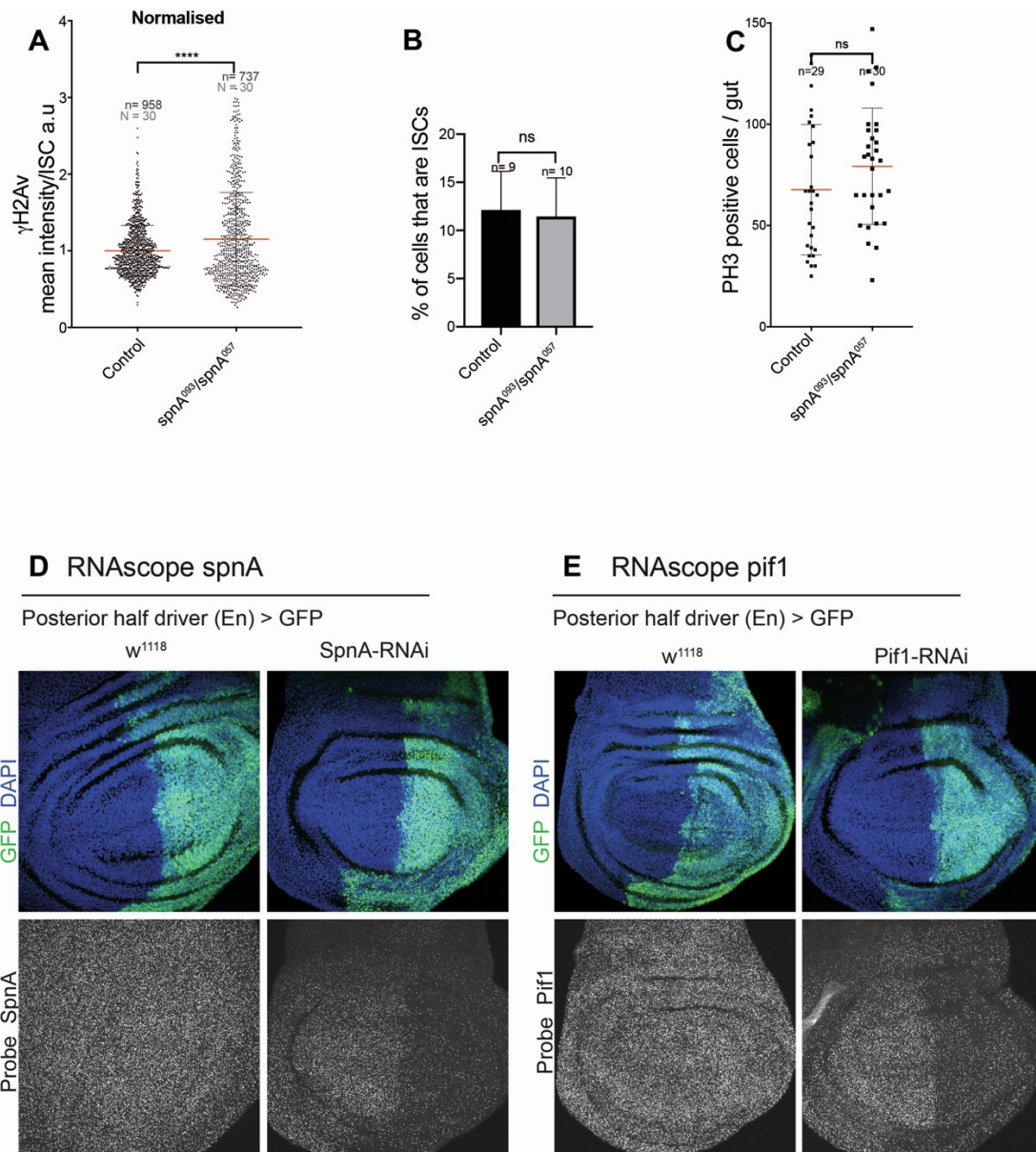


B'



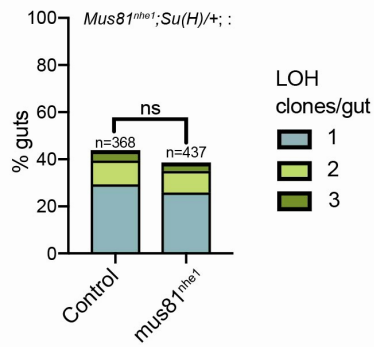
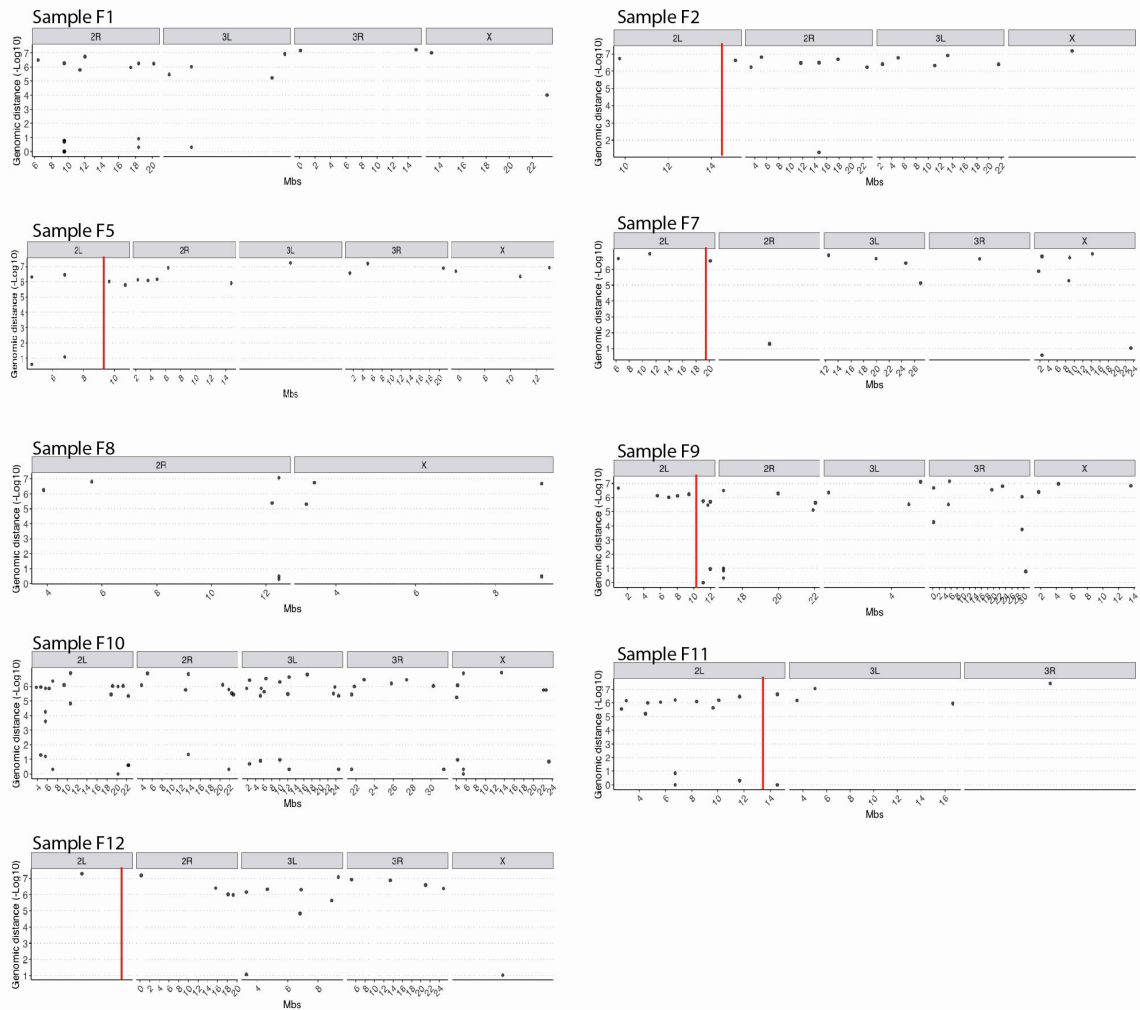
Supplementary Figure 3 (related to Figure 3): VAF plots of all the male samples

Plots of all male samples, showing all chromosomes. Only sample M1 (**A-A'**) shows that chromosome 2L has undergone an LOH event, with SNPs becoming homozygous (VAF >0.75). The remaining samples (**B-B'**) show no LOH on Chr 2L (left panels) but rather show a structural variants (SV) spanning the *Notch* locus on the X chromosome (right panels). DEL is deletion, BND indicates "break-end class" of genomic aberration.



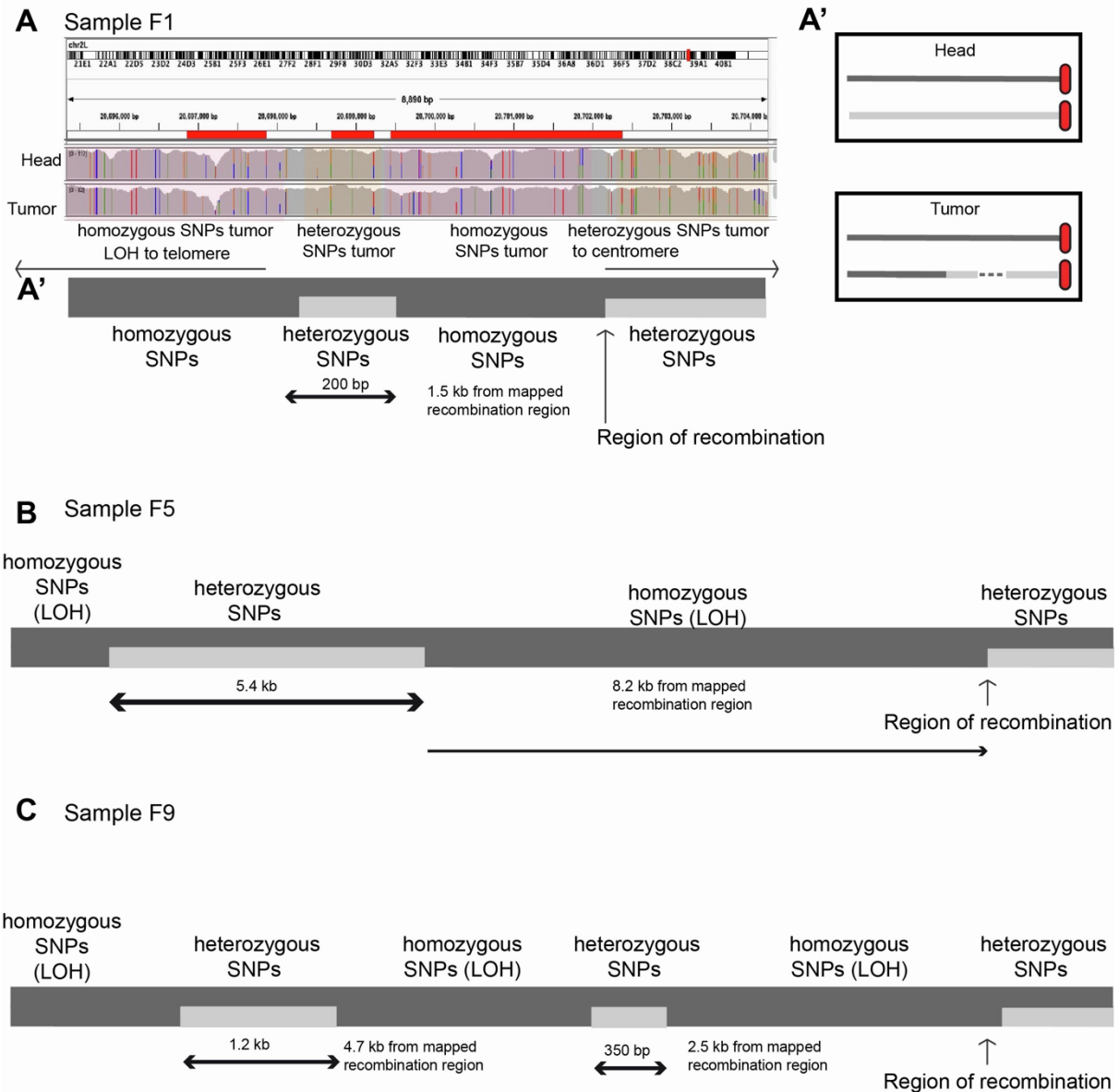
Supplementary Figure 4 (related to Figure 6): Characteristics of *spnA* mutants and *spnA* and *Pif1* knockdown

(A) Comparison of γ H2Av mean intensity (normalized arbitrary units) in ISCs of control or *spnA*⁰⁹³/*spnA*⁰⁵⁷ transheterozygous background at 5 weeks of age, t-test with Welch's correction. **(B)** No significant difference in percent ISCs per region of interest (ROI, corresponding to images of R4 and R2 portions of the guts) between control guts and *Su(H)*^{D47/+}; *SpnA*⁰⁹³/*SpnA*⁰⁵⁷ dissected at 5 weeks of age (t-test with Welch's correction). **(C)** No significant difference in number of mitotic cells per gut between control guts and *Su(H)*^{D47/+}; *SpnA*⁰⁹³/*SpnA*⁰⁵⁷ guts at 5 weeks of age (t-test with Welch's correction). **(E)** Validation of *spnA* RNAi knockdown efficiency using RNAscope: Wing disc expressing RNAi targeting *spnA* in the engrailed domain (marked by GFP). RNAscope using anti-*spnA* probe shows a reduction where RNAi (right panels) is expressed but not in controls that do not express RNAi (left panels). **(F)** Validation of *pif1* RNAi knockdown efficiency using RNAscope: Wing disc expressing RNAi targeting *pif1* in the engrailed domain (marked by GFP). RNAscope using anti-*pif1* probe shows a reduction where RNAi is expressed (right panels) is expressed but not in controls that do not express RNAi (left panels).

A**B**

Supplementary Figure 5 (related to Figure 6): Genetic and genomic data arguing against a BIR model.

(A) Percentage of LOH clones in *Mus81^{nhe1}; Su(H)^{D47/+}* compared with *+/+; Su(H)^{D47/+}*; control (Fisher's exact test, two-tailed). (B) Rainfall plots of point mutations in the sequenced LOH samples. Each point represents the genomic distance between two SNVs (point mutations). A mutational pileup would be detected by an accumulation of points vertically. We observed no mutational hotspots on chromosome 2L, arguing against a BIR model. Samples and chromosome arms not shown had no SNVs. Red line denotes approximate location of mapped site beginning of LOH, when mapping was possible (F10 could not be mapped due to EC purity).



Supplementary Figure 6 (related to Figures 4 and 6): Schematic showing samples with conversion tracts

(A) IGV view showing SNP evidence of a conversion tract 1.5 kb away from the mapped region of recombination. While the control head sample representing the germline (top IGV tract) shows all heterozygous SNPs, the bottom LOH tumor sample shows a shift from heterozygous to homozygous SNPs, then goes from homozygous to heterozygous, before going back from heterozygous to homozygous throughout the chromosome arm. A schematic of the cell of origin in head and tumor is shown on the right panel **A'**. **(A')** Schematic of sample F1 conversion tract denoted by shift from homozygous to heterozygous SNPs in the tumour sample for ~200 bp before again becoming homozygous until the telomere. **(B)** Schematic of sample F5: After the initial recombination site (indicated by arrow) there is a shift from heterozygous -> homozygous SNPs in the tumor, a region approximately 8.2 kb away showed a DNA tract marked by a shift from homozygous -> heterozygous SNPs for ~5.4 kb before again becoming homozygous until the telomere. **(C)** Schematic of sample F9 where 2 tracts were identified having heterozygous SNPs within the larger LOH region. Approximate length of each segmented is noted.

Supplementary Table 1: Coverage and purity of sequenced samples

For each pair of samples (intestinal neoplasia/tumor and paired head sample), the coverage and estimated purity is given along with the library preparation method. Red samples were excluded from further analysis due to low sequencing coverage in the tumor. In blue samples, SNPs indicated mitotic recombination, however mapping of recombination site was not possible due to contaminating surrounding enterocyte cells. Sample F28, in orange had no signs of mitotic recombination.

Supplementary Table 2: Mapped regions of recombination

For each tumor sample where mapping was possible, the approximate site of recombination is noted along with the resolution based on informative SNPs. Additionally, more complex cases with intervening heterozygous SNPs are noted.